Sequential and γ-secretase-dependent processing of the betacellulin precursor generates a palmitoylated intracellular-domain fragment that inhibits cell growth

Alexander Stoeck[1], Li Shang[1] and Peter J. Dempsey[1,2,*]

[1]Department of Pediatrics and Communicable Diseases, and [2]Department of Molecular and Integrative Physiology, University of Michigan, Ann Arbor, MI 48109, USA

*Author for correspondence (petedemp@med.umich.edu)

Accepted 13 April 2010
Journal of Cell Science 123, 2319-2331

doi:10.1242/jcs.060830

Summary

Betacellulin (BTC) belongs to the family of epidermal growth factor (EGF)-like growth factors that are expressed as transmembrane precursors and undergo proteolytic ectodomain shedding to release soluble mature ligands. BTC is a dual-specificity ligand for ErbB1 and ErbB4 receptors, and can activate unique signal-transduction pathways that are beneficial for the function, survival and regeneration of pancreatic β-cells. We have previously shown that BTC precursor (proBTC) is cleaved by ADAM10 to generate soluble ligand and a stable, transmembrane remnant (BTC-CTF). In this study, we analyzed the fate of the BTC-CTF in greater detail. We demonstrated that proBTC is cleaved by ADAM10 to produce BTC-CTF, which then undergoes intramembrane processing by presenilin-1- and/or presenilin-2-dependent γ-secretase to generate an intracellular-domain fragment (BTC-ICD). We found that the proBTC cytoplasmic domain is palmitoylated and that palmitoylation is not required for ADAM10-dependent cleavage but is necessary for the stability and γ-secretase-dependent processing of BTC-CTF to generate BTC-ICD. Additionally, palmitoylation is required for nuclear-membrane localization of BTC-ICD, as demonstrated by the redistribution of non-palmitoylated BTC-ICD mutant to the nucleoplasm. Importantly, a novel receptor-independent role for BTC-ICD signaling is suggested by the ability of BTC-ICD to inhibit cell growth in vitro.

Key words: Betacellulin, ADAM10, Regulated intramembrane proteolysis, Palmitoylation, Reverse signaling

Introduction

All epidermal growth factor (EGF)-receptor family (ErbB) ligands are synthesized as membrane-anchored precursors containing an N-terminal extracellular domain, a transmembrane domain and a cytoplasmic domain. In each ErbB-ligand precursor, the EGF-like domain, which confers ErbB-receptor binding and activation, is located next to the juxtamembrane stalk region of the extracellular domain and must be proteolytically cleaved to release soluble, active ligand (Citri and Yarden, 2006; Ohtsu et al., 2006; Sanderson et al., 2006b; Yarden, 2001). The principal sheddases responsible for this cleavage event are TNFα-converting enzyme (TACE; also known as ADAM17) and ADAM10, which belong to the disintegrin and metalloproteases family (ADAMs) (Blobel, 2005; Dempsey et al., 2002; Dong et al., 1999b; Peschon et al., 1998; Sahin et al., 2004; Sanderson et al., 2004; Sanderson et al., 2006b; Sunnarborg et al., 2002). Several in vivo experimental approaches, including ADAM17 loss-of-function and 'knock-in' studies of non-cleavable ErbB ligands in mice, have demonstrated that ectodomain shedding is an essential regulatory step for ErbB ligands to achieve full biological activity (Dempsey et al., 2002; Dong et al., 1999a; Peschon et al., 1998; Yamazaki et al., 2003). Moreover, the presence of a ready releasable pool of ErbB ligand at the cell surface, combined with the highly regulated nature of ADAM-mediated ErbB-ligand shedding, provides exquisite control over the temporal and spatial presentation of ligands to receptor populations (Blobel, 2005; Dempsey et al., 2002; Sanderson et al., 2006b). This feature of ErbB-ligand shedding also provides a mechanism to sense the local cellular environment, as highlighted by the ability of diverse extracellular signals to stimulate ADAM-dependent ErbB-receptor transactivation and thereby achieve the appropriate intracellular responses (Ohtsu et al., 2006).

For individual ErbB-ligand precursors, there is also substantial evidence that the membrane-anchoring and cytoplasmic domains can modulate ligand bioactivity and receptor presentation. For example, the cytoplasmic domains of several ErbB-ligand precursors regulate polarized trafficking and cell-surface expression (Brown et al., 2001; Dempsey and Coffey, 1994; Dempsey et al., 2003; Dempsey et al., 1997; Dong and Wiley, 2000), whereas the membrane-anchoring domain of the HB-EGF precursor (proHB-EGF) can confer juxtacrine activity (Dong et al., 2005). Moreover, accessory proteins, such as CD9, that directly interact with the cytoplasmic domains of specific ErbB-ligand precursors can also modify ligand function (Franklin et al., 2005; Glogowska et al., 2008; Imhof et al., 2008; Klonisch et al., 2009; Pyka et al., 2005; Shi et al., 2000; Shum et al., 1994; Shum et al., 1996). In addition, other post-translational modifications of ErbB-ligand precursors, including phosphorylation and palmitoylation of the cytoplasmic domain, are likely to further modulate these protein interactions and signaling events (Shum et al., 1996; Wang et al., 2006).

The cytoplasmic domains of ErbB-ligand precursors have also been implicated in 'reverse' receptor-independent signaling, which acts in a cell-autonomous manner. In the case of HB-EGF, a membrane-anchored HB-EGF cytoplasmic tail fragment (HB-EGF-CTF) generated by ectodomain shedding of proHB-EGF is translocated from the plasma membrane via retrograde endoplasmic reticulum (ER) trafficking to the nuclear envelope (Nanba et al., 2003). At the nucleus, HB-EGF-CTF can associate with and alter the activity of transcription factors such as promyelocytic leukemia

Journal of Cell Science

zinc finger (PLZF) (Kinugasa et al., 2007; Nanba et al., 2003). In addition, specific proHB-EGF isoforms, which retain the extracellular EGF-like domain, can also traffic to the inner nuclear membrane (INM) and modulate transcriptional activity (Hieda et al., 2008). Similarly, select amphiregulin precursor (proAR) isoforms can translocate from the plasma membrane to the INM owing to novel C-terminal processing and activation of a retrograde ER-retrieval signal (Isokane et al., 2008). These truncated proAR isoforms are maintained at the INM through protein interactions with A-type lamins and can regulate global transcription. However, in contrast to HB-EGF-CTF, AR-CTF has no reverse signaling capacity and is rapidly degraded in lysosomes (Isokane et al., 2008).

Another important mechanism for modulating cellular responses is the ability of membrane-anchored proteins such as Notch and ErbB4 receptor to undergo regulated intramembrane processing (RIP) to create soluble intracellular domains (ICDs) that regulate transcriptional activity (Selkoe and Kopan, 2003; Wolfe and Kopan, 2004). In most cases, RIP is a two-step process that involves metalloprotease-dependent ectodomain cleavage to generate a membrane-anchored CTF, followed by intramembrane processing via presenilin-dependent γ-secretase activity to produce a soluble ICD (Selkoe and Kopan, 2003; Wolfe and Kopan, 2004). Recently, it was reported that the ErbB ligand neuregulin precursor (proNRG-1) is also cleaved by γ-secretase activity and the released ICD (NRG-1-ICD) enters the nucleus and represses transcription of apoptotic regulators (Bao et al., 2003). Taken together, these findings suggest that select ErbB-ligand precursors are engaged in receptor-independent 'reverse' signaling, although the mechanisms for CTF and/or ICD generation and nuclear localization seem to be distinct (Higashiyama et al., 2008).

Another ErbB ligand, betacellulin (BTC), was originally isolated from rat insulinoma cells and can activate both ErbB1 and ErbB4 receptors (Dunbar and Goddard, 2000; Dunbar et al., 2001; Riese et al., 1996; Sweeney et al., 2000). We have previously demonstrated that the extracellular domain of proBTC can be proteolytically cleaved by ADAM10 to release the mature, active ligand and to produce a stable, cellular BTC remnant (termed BTC-CTF) (Moss et al., 2007; Sanderson et al., 2006a; Sanderson et al., 2005). Because of its stability, BTC-CTF represents a significant proportion of the cellular BTC isoforms expressed in cells under steady-state conditions. In this study, we sought to characterize the biological significance of BTC-CTF. We found that proBTC undergoes sequential ectodomain cleavage by ADAM10 to produce BTC-CTF, which is then susceptible to intramembrane processing by presenilin-1- and/or presenilin-2 (presenilin1/2)-dependent γ-secretase to generate an ICD fragment (BTC-ICD). Surprisingly, the proBTC cytoplasmic domain is palmitoylated and therefore the BTC-ICD remains associated with the membrane compartment and is localized to the nuclear membrane. Moreover, we demonstrated using a palmitoylation-deficient proBTC mutant that palmitoylation is important for the stability and γ-secretase-dependent processing of BTC-CTF to generate BTC-ICD. In addition, overexpression of a palmitoylated-BTC reporter construct (BTC-ΔE), which lacks the extracellular domain of proBTC but can still generate the BTC-ICD, inhibited cell proliferation in several different cell lines. Thus, proBTC is capable of regulated intramembrane processing and palmitoylation is a crucial post-translational modification involved in this process. Importantly, these observations provide the first evidence that BTC-ICD can engage in receptor-independent reverse signaling.

Results

BTC precursor is sequentially processed to generate a soluble BTC ligand and a membrane-anchored cytoplasmic tail fragment

Under both constitutive and Ca^{2+}-stimulated conditions, we recently showed that the conditionally immortalized mouse pancreatic epithelial (IMPE) cell line stably expressing wild-type (WT) proBTC with a C-terminal hemagglutinin (HA) tag (BTC-WT) (supplementary material Fig. S1A) was capable of ADAM10-dependent BTC shedding and the generation of a stable, cellular BTC remnant (termed BTC-CTF) (Moss et al., 2007). To investigate the biological significance of the BTC-CTF in IMPE cells expressing BTC-WT (IMPE-BTC-WT), we first verified that proBTC was correctly processed to produce BTC-CTF (Moss et al., 2007; Sanderson et al., 2006a; Sanderson et al., 2005). As shown in supplementary material Fig. S1B, four cellular BTC isoforms (40-, 30-, 25- and 19-kDa forms) were detected. Each of these transmembrane BTC isoforms expresses the immunoreactive EGF-like region of the extracellular domain and the complete cytoplasmic domain, therefore representing unshed BTC precursors. By contrast, the cellular 12-kDa species represents the membrane-anchored BTC remnant, BTC-CTF, which is generated after ectodomain cleavage (Moss et al., 2007; Sanderson et al., 2006a; Sanderson et al., 2005).

To verify that the generation of BTC-CTF required ectodomain cleavage, we examined two different non-cleavable (NC) proBTC mutants, NC-8 and NC CD4. In the NC-8 mutant, the first eight amino acids of the juxtamembrane stalk region (including the ectodomain cleavage site) were deleted, whereas, in the NC CD4 mutant, the juxtamembrane stalk region was replaced with the non-cleavable stalk region of CD4 (Maddon et al., 1985; Suzuki et al., 1997) (supplementary material Fig. S1A). Although the cellular expression of NC-8 and NC CD4 were similar to BTC-WT (supplementary material Fig. S1B), both constitutive and Ca^{2+}-ionophore-induced BTC shedding were dramatically reduced for both mutants (supplementary material Fig. S1C,D). Importantly, there was a marked reduction in the production of BTC-CTF in both NC-8 and NC CD4 mutants, thus providing additional evidence that ectodomain cleavage of proBTC is required for the generation of BTC-CTF.

Detection of a faster-migrating BTC-ICD fragment

To further characterize BTC-CTF under basal conditions, cell lysates from IMPE-BTC-WT and IMPE-Vector-alone (control) cells were immunoprecipitated with anti-HA-antibody-conjugated agarose beads and proteins were analyzed by western blotting with anti-HA antibody. Under these experimental conditions, the BTC-CTF represented a major HA-immunoreactive species in IMPE-BTC-WT cells. Intriguingly, upon longer exposures, a less-abundant but faster-migrating BTC fragment was consistently detected (~10 kDa, termed BTC intracellular domain, BTC-ICD) (Fig. 1A). To confirm that the BTC-ICD could be detected in cells expressing endogenous BTC, we examined the human A431 cell line, which is known to express BTC. Because Ca^{2+}-ionophore A23187 treatment can induce proBTC cleavage (Moss et al., 2007; Sahin et al., 2004; Sanderson et al., 2006a; Sanderson et al., 2005), A431 cells were treated with A23187 in the presence or absence of the ADAM10-selective inhibitor GI254023X (GI) prior to western blotting with an anti-human BTC cytoplasmic-domain antibody (Sanderson et al., 2006a). Because of the low levels of endogenous BTC expressed in A431 cells, only the two predominant BTC

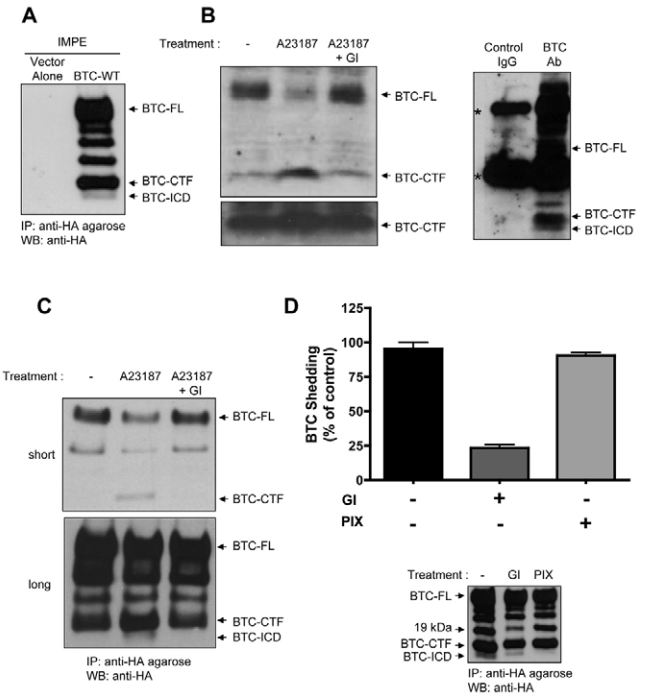

Fig. 1. Detection of a faster-migrating BTC-ICD fragment in IMPE-BTC-WT cells upon constitutive and Ca^{2+}-ionophore-induced BTC shedding. (**A**) Cell lysates were prepared from IMPE-BTC-WT and IMPE-Vector-alone (control) cells grown under serum-free conditions. (**B**) A431 cells were treated with or without the Ca^{2+} ionophore A23187 for 1 hour in the presence or absence of GI254023X (GI) prior to preparation of cell lysates. Left panel: cell lysates were directly analyzed by western blotting using an anti-human BTC cytoplasmic-domain antibody. Right panel: ionophore-induced A431 cell lysates were immunoprecipitated with control IgG or anti-BTC cytoplasmic-domain antibody prior to western blotting using the same antibody. Asterisks indicate IgG heavy (top) and light (bottom) chains. (**C**) IMPE-BTC-WT cells were treated with or without the Ca^{2+} ionophore A23187 for 1 hour in the presence or absence of GI254023X (GI) prior to preparation of cell lysates (upper panel: short exposure shows ionophore-induced ectodomain cleavage of BTC-FL and concomitant BTC-CTF production; lower panel: long exposure shows ionophore-induced generation of BTC-ICD). (**D**) IMPE-BTC-WT cells were treated overnight with or without metalloprotease inhibitor GI254023X or γ-secretase inhibitor PIX. CM was collected prior to preparation of cell lysates. Graph shows BTC shedding into CM, which was measured by BTC ELISA. Blot: all cellular BTC isoforms from IMPE cells were precipitated from cell lysates with anti-HA agarose and then analyzed in western blotting with anti-HA antibody.

isoforms, BTC-FL and BTC-CTF, were readily detected. Importantly, ionophore treatment stimulated BTC-FL cleavage and BTC-CTF production, whereas GI treatment blocked this processing. Unfortunately, it was difficult to clearly detect the BTC-ICD by this direct approach, even after very long exposures (Fig. 1B). To enhance detection of BTC-ICD, ionophore-induced A431 cell lysates were immunoprecipitated with the anti-BTC cytoplasmic-domain antibody prior to western blotting. Despite the IgG heavy and light chain (H&L) immunoreactive bands masking some of the BTC isoforms, both BTC-CTF and BTC-ICD isoforms could now be detected, confirming that this processing occurred with the endogenous WT BTC precursor (Fig. 1B).

Because of the extremely low levels of endogenous human BTC expressed in cell lines, the remaining studies were performed in IMPE cells overexpressing different tagged BTC constructs. To validate the results in A431 cells, the analysis of ionophore-induced BTC processing was repeated in IMPE-BTC-WT cells. In this case, enhanced generation of both BTC-CTF and BTC-ICD isoforms were detected and treatment with ADAM10-selective inhibitor GI blocked production of both BTC isoforms (Fig. 1C). Moreover, a direct comparison of the electrophoretic mobility of BTC-ICD with a C-terminally HA-tagged BTC cytoplasmic-domain construct that lacks the extracellular and transmembrane domains (BTC-ICD-Only) showed they had similar mobilities (supplementary material Fig. S2). Taken together, these results suggested that ADAM10-dependent proBTC shedding produces the cellular remnant BTC-CTF that is susceptible to further processing to generate the BTC-ICD.

ADAM10-mediated proBTC ectodomain cleavage is required for the generation of BTC-ICD

Several ADAM10-dependent substrates have been shown to undergo sequential processing by ADAM10 and presenilin-dependent γ-secretase activity to generate ICDs (Baron, 2003; Ferber et al., 2008; Riedle et al., 2009). To determine whether the generation of the BTC-ICD was dependent on proteolysis under constitutive conditions, IMPE-BTC-WT cells were treated with the ADAM10-selective inhibitor GI or the γ-secretase inhibitor IX (PIX) overnight. Consistent with our previous data (Moss et al., 2007), GI treatment efficiently blocked the release of BTC into the conditioned medium, whereas PIX treatment had no effect (Fig. 1D). However, GI only modestly reduced the generation of BTC-CTF and BTC-ICD, whereas the level of the 19-kDa proBTC isoform was considerably reduced, suggesting that the N-terminal processing of the proBTC ectodomain was also sensitive to GI inhibition (Fig. 1D). We have previously shown that the BTC-CTF has a remarkably long half-life (Sanderson et al., 2005). Thus, it is likely that the large, stable pool of BTC-CTF at steady state masks subtle changes in BTC-CTF production. Likewise, a similar explanation for the limited reduction of BTC-ICD levels after GI treatment can be made if BTC-ICD is directly generated from this same stable pool of BTC-CTF. Indeed, treatment of IMPE-BTC-WT cells with GI for 1 hour did not alter generation of BTC-ICD under constitutive conditions (data not shown; Fig. 2D). By contrast, overnight treatment with PIX completely blocked the generation of BTC-ICD but had no effect on the levels of the BTC-CTF or other cellular BTC isoforms (Fig. 1D).

To verify that ADAM10 was required for BTC-ICD generation, we examined constitutive proBTC processing in ADAM10-deficient and WT mouse embryonic fibroblast (MEF) cell lines stably transduced with BTC-WT. MEFs expressing BTC-WT were cultured overnight in the presence or absence of the ADAM10-selective inhibitor GI. As expected, WT MEFs efficiently released BTC into the conditioned medium (CM) and this was blocked with the GI inhibitor (Fig. 2A). By contrast, negligible BTC shedding was observed in ADAM10-deficient MEFs under all treatment conditions despite higher cellular proBTC expression compared with WT MEFs (supplementary material Fig. S3). Consistent with previous reports, these results confirm that ADAM10 is required for constitutive BTC shedding in MEFs (Sahin et al., 2004).

Similar to results in IMPE-BTC-WT cells, all previously described cellular BTC isoforms were detected in WT MEFs stably expressing BTC-WT. However, GI treatment blocked the generation of both BTC-CTF and BTC-ICD fragments more efficiently in WT MEFs expressing BTC-WT than in IMPE-BTC-WT cells,

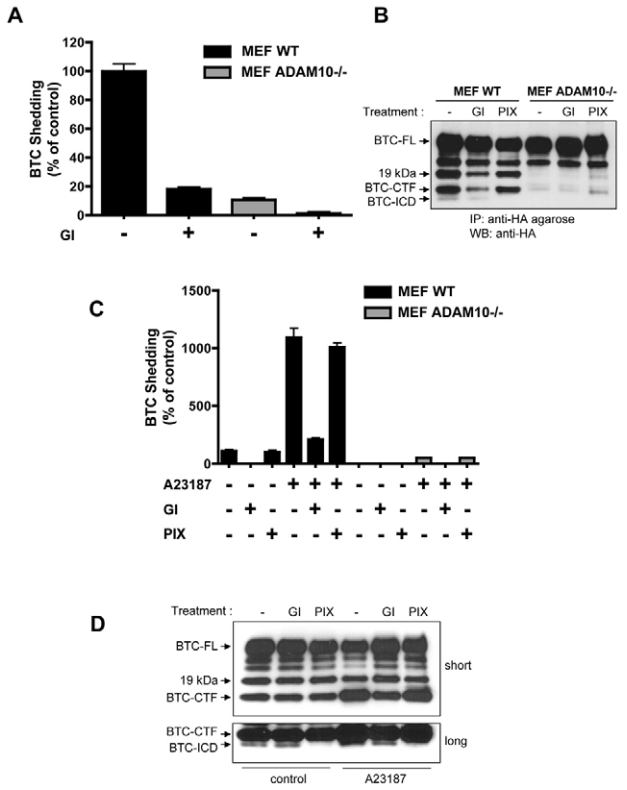

Fig. 2. ADAM10 is required for proBTC ectodomain cleavage and production of BTC-CTF and BTC-ICD. (**A**) WT MEFs or *ADAM10*$^{-/-}$ MEFs expressing proBTC were grown in serum-free DMEM for 24 hours in the presence or absence of GI254023X. BTC shedding into CM was measured by BTC ELISA. (**B**) WT MEFs and *ADAM10*$^{-/-}$ MEFs expressing proBTC were grown in serum-free DMEM for 24 hours in the presence or absence of GI254023X or PIX. Cell lysates were precipitated with anti-HA agarose and analyzed by western blot with anti-HA antibody. (**C**) WT MEFs or *ADAM10*$^{-/-}$ MEFs expressing proBTC were pre-incubated for 30 minutes in the presence or absence of GI254023X or PIX before treatment with or without A23187 for 1 hour. BTC shedding into CM was measured by BTC ELISA. (**D**) WT MEFs expressing proBTC were treated under the same conditions as in C. Cell lysates were precipitated with anti-HA agarose and analyzed by western blot with anti-HA antibody (upper panel: short exposure; lower panel: long exposure shows only BTC-CTF and BTC-ICD).

presumably because the rates of constitutive BTC shedding and BTC-CTF production are higher in WT MEFS (data not shown). However, PIX specifically inhibited generation of BTC-ICD in both cell lines (Fig. 2B). In ADAM10-deficient MEFs, only the full-length glycosylated proBTC (BTC-FL, 40-kDa isoform), immature proBTC precursor (30 kDa) and N-terminally processed proBTC (25 kDa) were readily detected. The 19-kDa BTC isoform, BTC-CTF and BTC-ICD were absent. The loss of the 19-kDa cellular isoform is also consistent with its observed GI sensitivity (Fig. 1C and Fig. 2B) and confirms that ADAM10 is involved in other proteolytic cleavage events outside of the juxtamembrane stalk region within the N-terminal region of the extracellular domain. Importantly, these findings demonstrate that, under constitutive conditions, ADAM10 activity is crucial for the generation of both BTC-CTF and BTC-ICD isoforms.

To determine whether Ca^{2+} influx can stimulate the generation of BTC-CTF and BTC-ICD in WT MEFs, we examined BTC ectodomain shedding after treatment with the Ca^{2+}-ionophore A23187. Ca^{2+} influx strongly enhanced release of soluble BTC from WT MEFs and the metalloprotease inhibitor GI blocked this shedding. The γ-secretase inhibitor PIX had no effect (Fig. 2C). Importantly, the Ca^{2+} ionophore did not induce significant BTC cleavage in ADAM10-deficient MEFs, confirming that ADAM10 is also required for ionophore-induced BTC shedding (Fig. 2C).

Similar to IMPE-BTC-WT cells under constitutive (1 hour) conditions, western blot analysis of cell lysates from WT MEFs expressing BTC-WT showed that the production of BTC-CTF and BTC-ICD were both insensitive to GI treatment. By contrast, GI blocked the enhanced production of both BTC-CTF and BTC-ICD after treatment with Ca^{2+} ionophore (Fig. 2D). Importantly, the γ-secretase inhibitor was capable of blocking the production of BTC-ICD under both, constitutive and ionophore-induced, conditions (Fig. 2D). As expected, the profile of BTC isoforms expressed in ADAM10-deficient MEFs was unaltered by Ca^{2+} influx (data not shown). These data indicate that ADAM10 plays a crucial role in the generation of BTC-CTF and BTC-ICD, but only the production of BTC-ICD is sensitive to γ-secretase inhibitors.

Presenilin-dependent γ-secretase activity is required for the generation of BTC-ICD

To determine whether presenilin-dependent γ-secretase activity was directly involved in the generation of BTC-ICD, BTC-WT was stably expressed in presenilin-1/2-deficient MEFs (PS1/2-BTC-WT). To verify that PS1/2-BTC-WT cells were still capable of ADAM10-dependent BTC shedding, cells were incubated for 1 hour under serum-free conditions or with A23187 in the presence or absence of the GI inhibitor as previously described. Similar to WT MEFs expressing BTC-WT, PS1/2-BTC-WT cells displayed efficient BTC shedding under both conditions that was still sensitive to GI inhibition (Fig. 3A). In addition, a similar pattern of cellular BTC isoforms, including BTC-CTF, was detected in PS1/2-BTC-WT MEFs, indicating that ADAM10 proteolytic activity was functional. However, unlike WT MEFs expressing BTC-WT, in which BTC-ICD was readily detected (Fig. 2B,D), BTC-ICD was absent in PS1/2-BTC-WT cells under all experimental conditions (Fig. 3B). These results demonstrate that BTC-WT is subject to sequential processing and that presenilin-dependent γ-secretase activity is required for the generation of BTC-ICD under constitutive and Ca^{2+}-ionophore-induced conditions.

BTC-ICD is generated at the plasma membrane and remains membrane bound owing to palmitoylation

To further characterize the cellular compartment in which BTC-CTF and BTC-ICD were produced, we monitored A23187-induced BTC shedding in homogenates from HEK293 cells expressing BTC-WT by sucrose-density centrifugation (Stoeck et al., 2006) (details available on request). At steady state, the majority of BTC-FL was detected at the plasma membrane. Upon stimulation with A23187, BTC-FL was rapidly converted to BTC-CTF and BTC-ICD. Intriguingly, newly generated BTC-CTF and BTC-ICD were also retained in the plasma-membrane compartment and subsequently were detected in early endosomes (supplementary material Fig. S4). The retention of BTC-ICD within membrane fractions was a surprising observation because most ICDs generated from other substrates are either rapidly degraded or released into the cytoplasm and translocated into the nucleus (Hass et al., 2009).

The predicted ICD of proBTC contains three cysteine residues closely juxtaposed to the inner leaflet of the plasma membrane that are potential sites for protein S-palmitoylation (see below).

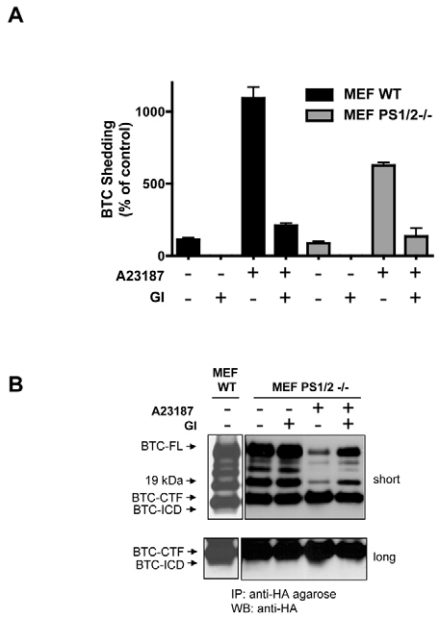

Fig. 3. Presenilin-1/2-dependent γ-secretase activity is required for generation of BTC-ICD. WT MEFs and presenilin-1/2-deficient MEFs expressing proBTC were pre-incubated for 30 minutes in the presence or absence of the inhibitor GI before stimulation with or without A23187. (**A**) BTC shed into CM was measured by BTC ELISA. (**B**) Cell lysates were precipitated with anti-HA agarose and analyzed by western blot with anti-HA antibody (upper panel: short exposure; lower panel: long exposure shows only BTC-CTF and BTC-ICD).

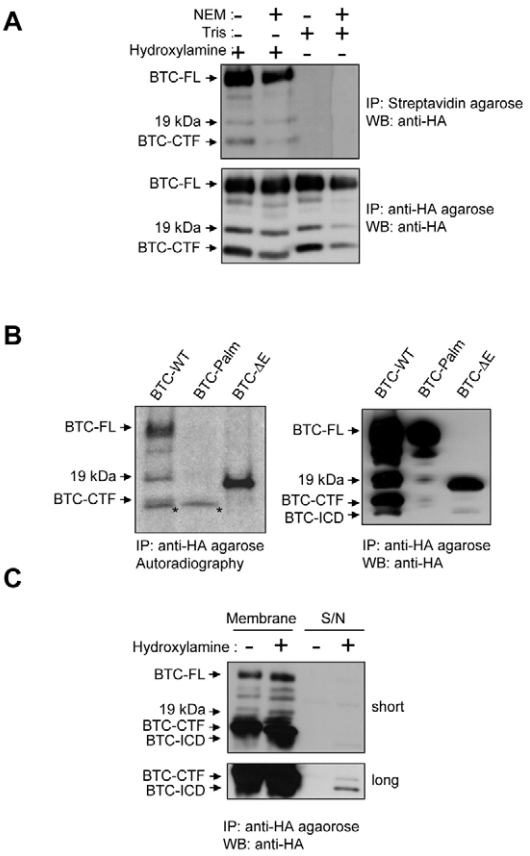

Fig. 4. BTC-ICD remains attached to the membrane compartment through palmitoylation. (**A**) IMPE-BTC-WT cells were lysed in lysis buffer with or without 50 mM NEM and cellular BTC isoforms precipitated with anti-HA agarose prior to acyl-biotin exchange labeling as described in the Materials and Methods. Eluted biotinylated proteins were re-precipitated with streptavidin-agarose and analyzed by western blot with anti-HA antibody (upper panel). Separate samples were directly analyzed in western blot with anti-HA antibody as loading controls (lower panel). (**B**) IMPE cells expressing either BTC-WT, BTC-Palm or BTC-ΔE were incubated in fatty-acid-free DMEM supplemented with 200 μCi of [^{3}H]palmitic acid for 6 hours at 37°C. Cell lysates were precipitated with anti-HA agarose and analyzed in western blot with anti-HA antibody (right panel) or membranes were used for autoradiography (left panel). (**C**) IMPE-BTC-WT cells were homogenized in the presence or absence of 1 M hydroxylamine-HCl (hydroxylamine) prior to pelleting membranes as described in the Materials and Methods. Cell lysates from membrane fractions and supernatants (S/N) were precipitated with anti-HA agarose and analyzed by western blotting with anti-HA antibody (upper panel: short exposure; lower panel: long exposure shows only BTC-CTF and BTC-ICD).

To investigate whether proBTC contains S-palmitoylation modifications that might influence its cellular localization, an S-palmitoylation-specific acyl-biotin exchange strategy was used (Drisdel et al., 2006; Drisdel and Green, 2004). Cell lysates from IMPE-BTC-WT cells were treated with or without N-Ethylmaleimide (NEM) to block free thiols prior to acyl-biotin exchange reaction labeling. Although pre-treatment with NEM did not affect accessibility of sulfhydryl-reactive biotin, only HA immunoprecipitates treated with hydroxylamine were labeled, indicating that proBTC can be modified by S-palmitoylation (Fig. 4A). Importantly, all cellular BTC isoforms were labeled except for the 30-kDa species, which probably represents an immature proBTC form within the early secretory compartment (Sanderson et al., 2005). Importantly, even though HA immunoprecipitates from all experimental conditions were readily detected by western blotting, all BTC isoforms from hydroxylamine-treated samples had faster electrophoretic mobilities compared with their untreated counterparts, providing further evidence that hydroxylamine-sensitive modifications had been removed from these proteins (Fig. 4A).

As further validation, IMPE-BTC-WT cells were labeled with [^{3}H]-palmitic acid, lysed and immunoprecipitated with anti-HA agarose beads. Autoradiography was performed to detect [^{3}H]-labeled BTC and total BTC immunoreactivity was detected by anti-HA western blotting. All cellular BTC isoforms previously labeled with acyl-biotin were also labeled with [^{3}H]-palmitic acid, confirming that proBTC is S-palmitoylated (Fig. 4B).

To investigate whether membrane association of BTC-ICD was due to palmitoylation, the above strategy was adapted to examine whether hydroxylamine could be used to release BTC-ICD from membrane fractions. Therefore, IMPE-BTC-WT cell homogenates were prepared in the presence or absence of hydroxylamine and centrifuged to pellet all membranes. HA immunoprecipitates were prepared from membrane and supernatant fractions. Only homogenates treated with hydroxylamine displayed BTC-ICD in the supernatant fraction. An important control for this experiment was that no significant amounts of any other cellular BTC isoforms were detected in the supernatant fraction, which is consistent with these other BTC isoforms being retained in the membrane fraction as transmembrane proteins (Fig. 4C). In summary, these findings suggest that membrane-anchored BTC-CTF is susceptible to γ-

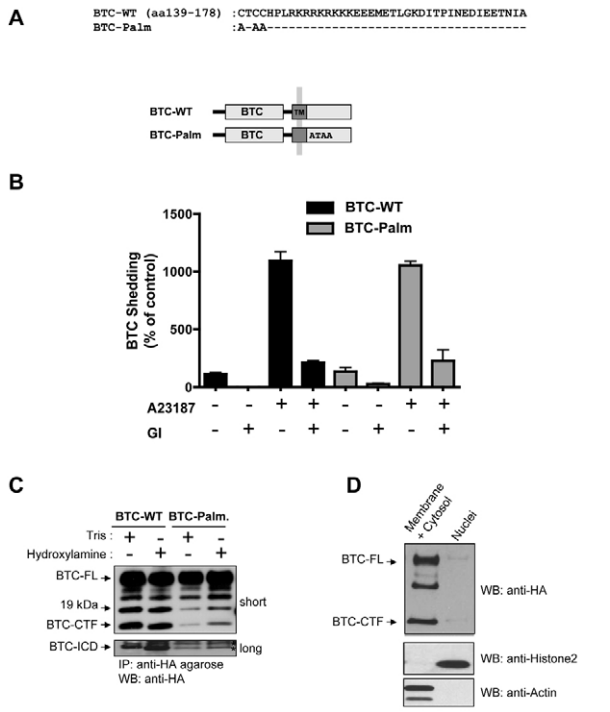

Fig. 5. Palmitoylation is required for stable production of BTC-ICD. (**A**) Amino acid sequence of BTC-WT cytoplasmic domain with potential palmitoylation sites (C139, C141 and C142), which were exchanged to alanines in the BTC-Palm mutant (upper panel). A schematic of BTC-WT and BTC-Palm constructs used in this study (lower panel). (**B-D**) IMPE cells expressing BTC-WT or BTC-Palm were pre-incubated in serum-free DMEM for 30 minutes in the presence or absence of GI inhibitor before treatment with or without A23187 for 1 hour. (B) BTC shed into the CM was measured by BTC ELISA. (C) Cell lysates were precipitated with anti-HA agarose and then treated with 1 M hydroxylamine-HCl (Hydroxylamine) or 1 M Tris (Tris) as described in the Materials and Methods, prior to western blotting with anti-HA antibody (upper panel: short exposure; lower panel: long exposure of BTC-ICD). Asterisks represent non-specific bands. (D) Nuclear and membrane/cytosolic fractions were isolated from IMPE-BTC-Palm cells and analyzed by western blot using anti-HA antibody. Actin (cytosol) and histone 2 (nuclear) levels were measured to ensure purity of fractions.

secretase cleavage to generate BTC-ICD and that BTC-ICD is retained at membranes through S-palmitoylation.

Palmitoylation of proBTC is required for the generation of BTC-ICD

To determine whether palmitoylation of proBTC is involved in sequential BTC processing, a mutant proBTC construct was generated in which all three cysteine residues that are potential sites for S-palmitoylation were replaced with alanine residues (termed BTC-Palm) (Fig. 5A). The inability of the BTC-Palm mutant to incorporate [^{3}H]-palmitic acid when expressed in IMPE cells confirmed that these residues, either individually or in combination, were the crucial sites responsible for S-palmitoylation modification (Fig. 4B). Because palmitoylation can influence protein trafficking and intracellular localization (Greaves and Chamberlain, 2007; Greaves et al., 2009), cellular distribution of BTC-WT and BTC-Palm was compared by immunofluorescence staining with an anti-BTC antibody directed against the extracellular domain. No significant differences in cellular distribution were observed (data not shown). To investigate whether palmitoylation affected proBTC shedding, IMPE-BTC-Palm cells were treated with or without A23187 in the presence or absence of GI. No differences in constitutive and ionophore-induced BTC shedding were observed with BTC-Palm as compared to BTC-WT (Fig. 5B). In addition, GI efficiently blocked BTC shedding under both conditions, suggesting that ADAM10-mediated BTC shedding is independent of palmitoylation (Fig. 5B).

To determine whether the BTC-Palm mutant can still generate the BTC-CTF and BTC-ICD, cellular BTC isoforms expressed in IMPE-BTC-Palm cells were compared with IMPE-BTC-WT cells. All transmembrane BTC isoforms expressed in IMPE-BTC-WT cells had similar counterparts in IMPE-BTC-Palm cells but there was a striking difference in the proportion of individual species. In particular, there was a significant decrease in the levels of BTC-CTF and to a lesser degree the 19-kDa isoform. More importantly, BTC-ICD was absent in IMPE-BTC-Palm cells even in the longest exposures (Fig. 5C; data not shown). Because the BTC-Palm mutant shows no defects in ectodomain shedding, these data suggest that non-palmitoylated BTC-CTF and BTC-ICD are less stable. Indeed, it has been difficult to maintain high expression of non-palmitoylated HA-tagged BTC-ICD-Only in cells (data not shown). However, we cannot rule out the possibility that the loss of BTC-ICD production is also due to the inability of non-palmitoylated BTC-CTF to be processed by γ-secretase activity. Interestingly, our attempts to block proteasomal degradation of BTC-ICD using proteasomal inhibitors have been hampered by the fact that these same inhibitors are also known to block γ-secretase activity (Ebinu and Yankner, 2002; Murakami et al., 2003; Steinhilb et al., 2001; Zhang et al., 1999). Further studies are therefore needed to address these possibilities; nevertheless, palmitoylation is a crucial modification for stable expression of BTC-CTF and BTC-ICD.

Non-palmitoylated BTC-ICD translocates to the nucleus

Several ErbB-ligand precursors can translocate to the nucleus by distinct mechanisms and influence gene expression (Bao et al., 2003; Hieda et al., 2008; Higashiyama et al., 2008; Isokane et al., 2008). To determine whether the BTC-ICD translocates to the nucleus, constructs encoding the ICD of BTC with N- or C-terminal EGFP tags were generated (BTC-ICD-Only). Both these constructs are predicted to be expressed in the cytoplasm and should not be palmitoylated (Fig. 6A). To determine the cellular localization of BTC-ICD-Only, IMPE cells expressing BTC-WT, BTC-ICD-Only or EGFP alone were analyzed by confocal microscopy. In IMPE cells expressing BTC-WT, EGFP fluorescence was primarily localized at the plasma membrane, although discernible, albeit weak, expression was observed in the nucleus. IMPE cells expressing EGFP alone were used as a control and showed EGFP localized diffusely throughout the cytoplasm and nucleus (Fig. 6B). By contrast, BTC-ICD-Only was strongly expressed in the nucleus and is associated with nucleoli (Fig. 6B) and with nuclear speckling in other cell types (supplementary material Fig. S5). The presence of BTC-ICD-Only in the nucleus was confirmed by western blot analysis of membrane and cytosolic (membrane/cytosolic) and nuclear fractions from IMPE-BTC-ICD-Only cells using an anti-EGFP antibody (Fig. 6C). Taken together, these data suggest that soluble, non-palmitoylated BTC cytoplasmic domain can traffic to the nucleus.

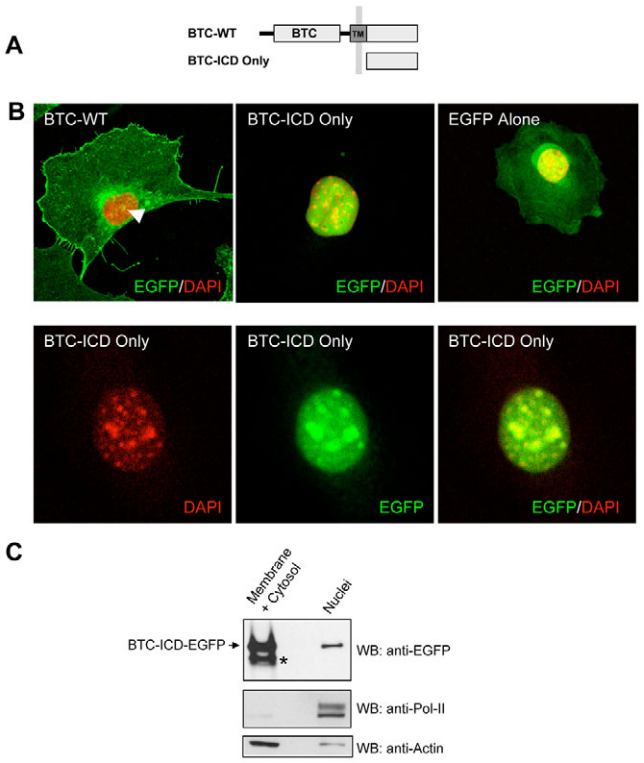

Fig. 6. Non-palmitoylated BTC-ICD-Only is localized to the nucleus. (**A**) A schematic of wild-type proBTC (BTC-WT) and BTC-ICD-Only, a construct generated by adding an ATG start codon at the N-terminus of the predicted BTC cytoplasmic domain. All constructs contained a C-terminal EGFP tag. (**B**) IMPE cells expressing BTC-WT, BTC-ICD-Only and EGFP alone were grown on glass coverslips, fixed and EGFP localized as described in the Materials and Methods. Upper panel: arrowhead indicates nuclear localization of EGFP in IMPE cells expressing BTC-WT (magnification 60×). Lower panel: a higher-magnification view of BTC-CD-Only staining in IMPE cells (magnification 120×). (**C**) Nuclear and membrane/cytosolic fractions were isolated from IMPE-BTC-ICD-Only cells and analyzed by western blot using anti-EGFP antibody. Actin (cytosol) and polymerase II (nuclear) levels were measured to ensure purity of fractions. Asterisk represents an additional EGFP immunoreactive band that is not expressed in the nuclear fraction.

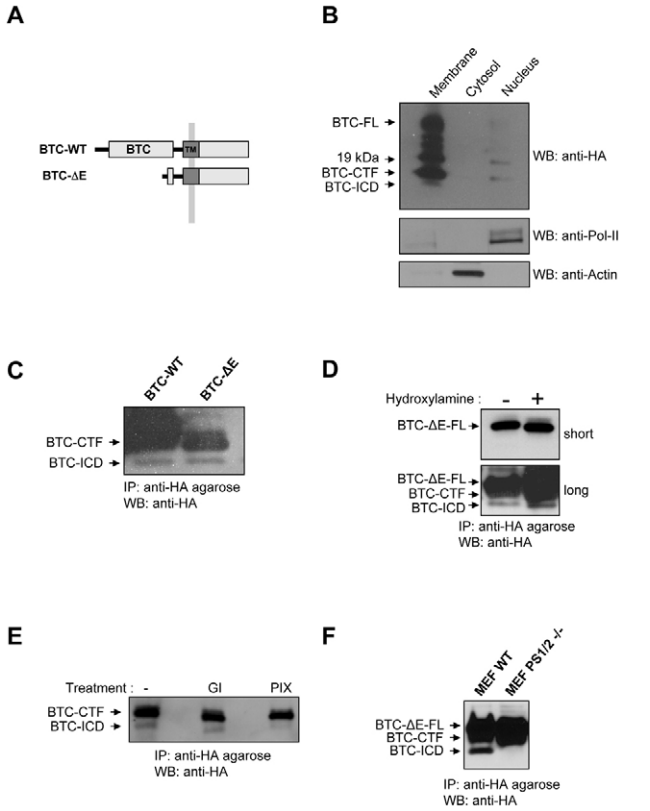

Fig. 7. BTC-ΔE mutant is palmitoylated and sequentially processed to generate BTC-CTF and BTC-ICD. (**A**) A schematic of BTC-WT and BTC-ΔE, a construct lacking the majority of the extracellular domain but still containing ADAM10- and γ-secretase-cleavage sites. (**B**) Nuclear, cytosolic and membrane fractions isolated from IMPE-BTC-WT cells were analyzed by western blot using anti-HA antibody. Actin (cytosol) and polymerase II (nuclear) levels were measured to ensure purity of fractions. (**C**) IMPE cells expressing BTC-WT or BTC-ΔE were lysed and precipitated with anti-HA agarose prior to western blotting with anti-HA antibody. (**D**) IMPE-BTC-ΔE cell lysates were precipitated with anti-HA agarose and then treated with or without 1 M hydroxylamine-HCl (hydroxylamine) prior to western blotting with anti-HA antibody (upper panel: short exposure; lower panel: long exposure). (**E**) IMPE-BTC-ΔE cells were incubated in serum-free DMEM with or without the inhibitors GI or PIX for 24 hours. Cells lysates were precipitated with anti-HA agarose and analyzed by western blot with anti-HA antibody. (**F**) WT MEFs and presenilin-1/2 (PS1/2)-deficient MEFs expressing BTC-ΔE were lysed and precipitated with anti-HA agarose prior to western blotting with anti-HA antibody.

Palmitoylated BTC-ICD is localized at the nuclear membrane

To determine whether palmitoylated BTC-ICD can translocate to the nucleus, nuclei and membrane/cytosolic fractions were purified from IMPE-BTC-WT cells and analyzed by anti-HA western blotting. As expected, BTC-ICD was detected in the membrane fraction and a small, but consistent, amount of BTC-ICD immunoreactivity was detected within the nuclear fraction (Fig. 7B). No BTC-ICD was detected in the cytosol. Interestingly, low levels of the 19-kDa transmembrane BTC isoform were also detected in the nuclear fraction. Furthermore, the inability to detect BTC isoforms in the nuclear fractions from IMPE-BTC-Palm cells suggested that palmitoylation modifications might be involved in nuclear trafficking (Fig. 5D). However, because the relatively low levels of BTC-ICD in the nucleus from IMPE-BTC-WT cells (Fig. 6B and Fig. 7B) hindered detailed analysis of its cellular localization, we sought an alternative strategy to express palmitoylated BTC-ICD in cells.

To further characterize the cellular localization and function of BTC-ICD, a BTC construct was generated that lacked most of the extracellular domain but retained the predicted ADAM10-cleavage site, transmembrane domain (including the γ-secretase-cleavage site) and the ICD with a C-terminal HA-tag (BTC-ΔE) (Fig. 7A). A similar construct has been used to study the role of Notch1-ICD and led to the generation of constitutively active Notch1-ICD (Mumm et al., 2000).

To investigate whether BTC-ΔE is still sequentially processed, the cellular BTC isoforms in IMPE-BTC-ΔE cells were compared to IMPE-BTC-WT cells. Consistent with the BTC-ΔE mutant lacking most of the extracellular domain, only a single full-length species (BTC-ΔE-FL, ~20 kDa), BTC-CTF and BTC-ICD were generated. Importantly, both BTC-CTF and BTC-ICD had similar electrophoretic mobilities to their WT counterparts (Fig. 7C). In addition, all cellular BTC-ΔE isoforms were labeled with [^{3}H]-

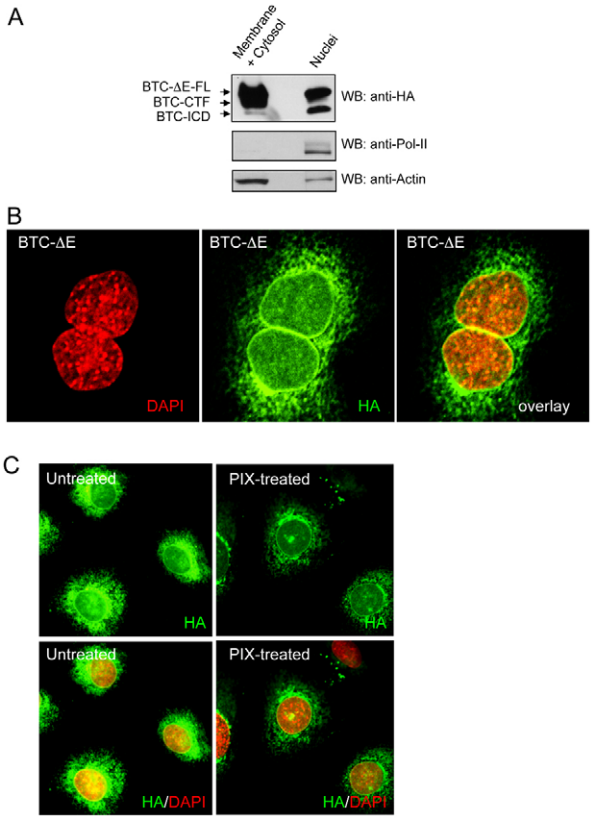

Fig. 8. Palmitoylated BTC-ICD is localized to the nuclear membrane. (**A**) Nuclear and membrane/cytosolic fractions isolated from IMPE-BTC-ΔE cells were analyzed by western blot using anti-HA antibody. Actin (cytosol) and polymerase II (nuclear) levels were measured to ensure purity of fractions. (**B**) IMPE-BTC-ΔE cells were grown on glass coverslips, fixed and BTC-ΔE immunolocalized using anti-HA antibody as described in the Materials and Methods (magnification 120×). (**C**) IMPE-BTC-ΔE cells were grown on glass coverslips and incubated overnight in serum-free DMEM with or without the γ-secretase inhibitor PIX prior to immunostaining as described above (magnification 60×).

palmitic acid and were sensitive to hydroxylamine, suggesting that the BTC-ΔE mutant can undergo S-palmitoylation (Fig. 4B and Fig. 7D). Furthermore, the generation of BTC-ICD in IMPE-BTC-ΔE cells was reduced by treatment with the inhibitors GI or PIX, indicating that the construct was still susceptible to sequential processing (Fig. 7E). Importantly, no BTC-ICD was detected when the BTC-ΔE mutant was expressed in presenilin-1/2-deficient cells (Fig. 7F).

To study the cellular localization of BTC-ICD in IMPE-BTC-ΔE cells, nuclei and membrane/cytosolic fractions were prepared and analyzed as previously described. Full-length BTC-ΔE and BTC-CTF were primarily detected in the membrane fraction, whereas BTC-ICD was weakly expressed in this fraction. Significantly, the majority of BTC-ICD was detected in the nuclear fraction (Fig. 8A). In addition, a smaller amount of the full-length BTC-ΔE, but no BTC-CTF, was detected in the nuclear fraction (Fig. 8A).

To visualize the cellular localization of BTC-ΔE, IMPE-BTC-ΔE cells were stained with anti-HA antibody and then examined by confocal microscopy. BTC-ΔE immunoreactivity was present in the Golgi and plasma membrane but surprisingly it was strongly localized to the nuclear membrane and only weak immunoreactivity was observed in the nucleus (Fig. 8B). This localization is quite distinct from the intranuclear localization observed with non-palmitoylated BTC-ICD-Only (Fig. 6B). When IMPE-BTC-ΔE cells were treated with the γ-secretase inhibitor PIX, the intensity of HA immunoreactivity was reduced at the nuclear membrane and at the same time enhanced in the Golgi and plasma-membrane compartments (Fig. 8C). We speculate that the residual immunoreactivity in the nuclear fraction might be associated with full-length BTC-ΔE that had been detected biochemically in the nuclear fraction; this is also consistent with recent reports for nuclear trafficking of other ErbB ligands (Hieda et al., 2008; Higashiyama et al., 2008; Isokane et al., 2008). Thus, the palmitoylated BTC-ICD, unlike the non-palmitoylated version, is primarily localized to the nuclear membrane rather than trafficking into the nucleus.

Overexpression of BTC-ΔE inhibits cell growth

The cytoplasmic domains of several other ErbB-ligand precursors have been implicated in transcriptional regulation and cell-cycle progression (Hieda et al., 2008; Higashiyama et al., 2008). To investigate whether the BTC-ICD had growth-regulatory properties, we examined the growth responses of BTC-WT, secreted BTC (a constitutively secreted BTC form termed BTC-Sec) (supplementary material Fig. S6) and BTC-ΔE stably expressed in IMPE cells, and compared them to IMPE cells stably expressing control expression vector (IMPE-Vector-alone). In IMPE cells, BTC-WT enhanced cell growth by ~150% compared with control cells (Fig. 9A), whereas IMPE-BTC-Sec cells displayed a positive but weaker growth response despite releasing more BTC than IMPE-BTC-WT cells (supplementary material Fig. S6). By contrast, BTC-ΔE inhibited cell growth by ~45% compared with IMPE-Vector-alone cells (Fig. 9B). These data suggest that sequential processing of proBTC generates both stimulatory and inhibitory growth signals through the generation of soluble BTC ligand and the BTC-ICD, respectively.

Discussion

Recent studies have demonstrated that several ErbB-ligand precursors, including HB-EGF, AR and NRG-1, can engage in two distinct signal-transduction pathways associated with their respective extracellular and intracellular domains (Higashiyama et al., 2008). The first pathway is a classical receptor-dependent pathway that involves ectodomain cleavage of the growth-factor precursor to generate a soluble ligand that can activate ErbB receptors. The second pathway is receptor independent, termed reverse signaling, and involves nuclear localization and signaling by the ICD of the ligand precursor (Higashiyama et al., 2008). Although the mechanisms for production and nuclear trafficking of each ICD seem to be distinct, a common feature of reverse signaling is the transcriptional regulation of gene expression (Bao et al., 2004; Bao et al., 2003; Hieda et al., 2008; Higashiyama et al., 2008; Isokane et al., 2008; Nanba et al., 2003). In the present study, we show that the BTC precursor (proBTC) can undergo sequential processing by ADAM10 and presenilin1/2-dependent γ-secretase to generate BTC-ICD. Furthermore, proBTC is palmitoylated and this post-translational modification is required for the stability and γ-secretase-dependent processing of the BTC-CTF to generate BTC-ICD. Intriguingly, palmitoylation is also required for localization of BTC-ICD to the nuclear membrane, as

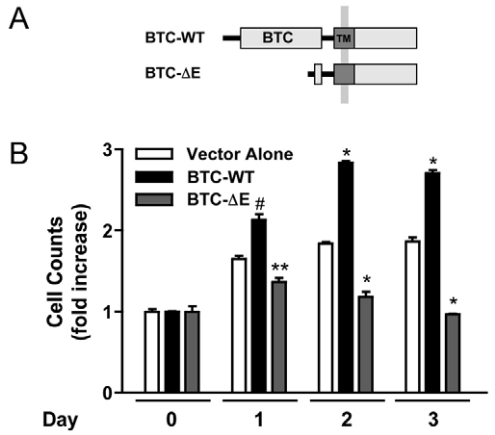

Fig. 9. Overexpression of BTC-ICD inhibits cell growth. (**A**) A schematic of wild-type proBTC (BTC-WT) and BTC-ΔE used in this study. All constructs contain a C-terminal HA-tag. (**B**) A comparison of growth responses between IMPE cells expressing BTC-WT, BTC-ΔE or control (vector alone). All cell lines were plated at 5×10^4 cells per well and cell counts were normalized to plating efficiency after 24 hours. Statistical analysis (unpaired Student's *t*-test) was performed between IMPE-Vector-alone and IMPE-BTC-WT or IMPE-Vector-alone and IMPE-BTC-ΔE at each time point. *P*-values were: #, $P=0.0008$; **$P=0.0045$ and *$P<0.0001$.

demonstrated by the redistribution of non-palmitoylated BTC-ICD mutant to the nucleoplasm. Importantly, a novel receptor-independent role for BTC-ICD signaling is suggested by the ability of BTC-ICD to inhibit cell growth in vitro.

It has been postulated that the primary housekeeping function of RIP is to control cellular levels of membrane-anchored proteins by removing unwanted transmembrane-protein remnants and the soluble ICDs that are released into the cytosol undergo proteasomal degradation. Similarly, transmembrane proteins such as Notch and ErbB4 that undergo RIP to generate soluble ICDs involved in intracellular signaling require translocation of the soluble ICD through the cytosol into the nucleus (Hass et al., 2009). It was therefore surprising to find that, after generation of BTC-ICD at the plasma membrane, BTC-ICD was not detected in the cytosol but remained associated with the membrane compartment, despite lacking a predicted transmembrane domain. This was an intriguing observation and led to the discovery that the proBTC cytoplasmic domain is S-palmitoylated. The ability of hydroxylamine treatment to release only BTC-ICD, but no other cellular BTC isoforms, including BTC-CTF, from membrane fractions, confirmed that the S-palmitoylation modification was responsible for the membrane attachment of BTC-ICD. To our knowledge, proTGFα is the only other ErbB-ligand precursor to contain S-palmitoylation modifications (Shum et al., 1996), but unlike BTC, it is not currently known whether proTGFα is susceptible to RIP-mediated processing.

Palmitoylation is a reversible post-translational modification that is known to regulate protein stability and trafficking between distinct subcellular membrane compartments (Greaves and Chamberlain, 2007; Greaves et al., 2009; Linder and Deschenes, 2006; Linder and Deschenes, 2007). How might this post-translational modification affect proBTC and its regulated intramembrane processing? Intriguingly, our data suggest that S-palmitoylation of proBTC might act on several levels to regulate the production and localization of BTC-ICD. Several lines of evidence have implicated detergent-resistant microdomains (DRMs) as the cellular location of functional γ-secretase activity. For example, some γ-secretase subunits, including activated presenilin, have high affinity for DRMs (Vetrivel et al., 2005; Vetrivel et al., 2004). In addition, a number of γ-secretase substrates, such as APP and neurotrophin receptor ($p75^{NTR}$), are localized to DRMs and processing of γ-secretase substrate can be inhibited by cholesterol depletion (Gil et al., 2007; Matthews et al., 2003; Underwood et al., 2008; Urra et al., 2007; von Tresckow et al., 2004). Conversely, in cells lacking γ-secretase activity, ectodomain cleavage of APP generated a CTF that accumulated in lipid rafts, inferring that subsequent γ-secretase processing takes place within DRMs (Vetrivel et al., 2005). A recent study showed that two subunits of the γ-secretase complex, APH-1 and nicastrin, are S-palmitoylated and that palmitoylation plays a role in both stability and raft localization of the γ-secretase complex (Cheng et al., 2009). However, palmitoylation-deficient APH-1 and nicastrin could still assemble into a functional γ-secretase complex capable of intramembrane processing (Cheng et al., 2009). Although palmitoylation of the γ-secretase complex is apparently not essential for RIP activity, the opposite conclusion was drawn for the γ-secretase substrate $p75^{NTR}$, which is another palmitoylated protein (Underwood et al., 2008). Interestingly, ADAM17-mediated shedding of $p75^{NTR}$ does not require lipid microdomains or palmitoylation and is enhanced by cholesterol depletion (Gil et al., 2007; Matthews et al., 2003; Underwood et al., 2008), whereas the $p75^{NTR}$-CTF must be palmitoylated for translocation to cholesterol-rich domains and subsequent intramembrane processing to generate the ICD (Underwood et al., 2008). Similarly, we find that proBTC palmitoylation is not required for ADAM10-dependent ectodomain shedding but palmitoylation is required for presenilin-dependent γ-secretase processing of BTC-CTF to generate BTC-ICD. These studies suggest that palmitoylation is needed for efficient or stable recruitment of substrate proteins into microdomains associated with γ-secretase activity. The recent demonstration that ADAM10 can also undergo RIP further underscores the complex nature of the physical relationship between substrates, ADAM sheddases and downstream γ-secretase complexes in these membrane compartments (Parkin and Harris, 2009; Tousseyn et al., 2009).

Despite efficient ectodomain shedding, the marked reduction in BTC-CTF levels observed in the proBTC palmitoylation-deficient mutant (BTC-Palm) suggests that palmitoylation might also directly influence the stability of both BTC-CTF and BTC-ICD. Similar to AR-CTF (Isokane et al., 2008), non-palmitoylated BTC-CTF might be rapidly endocytosed and sent for lysosomal degradation, reducing the cellular pool of BTC-CTF available to generate BTC-ICD. Alternatively, non-palmitoylated BTC-CTF might still be subject to γ-secretase activity but its cytosolic BTC-ICD counterpart might be less stable owing to proteasomal degradation. To determine whether BTC-CTF and/or BTC-ICD are rapidly degraded in this way, we treated cells with different concentrations of proteasome inhibitors MG132 and the proteasome inhibitor-1, but did not see an accumulation of either BTC-CTF or BTC-ICD (data not shown). Several proteasome inhibitors, including MG132, can inhibit γ-secretase activity (De Strooper et al., 1999; Murakami et al., 2003), which might be expected to block BTC-ICD production and accumulate BTC-CTF; however, this was not observed (data not shown). Although the potential roles of palmitoylation in protein stability and γ-secretase activity are not mutually exclusive, further studies are needed to determine their respective contributions to the loss of BTC-CTF and BTC-ICD in the proBTC

palmitoylation-deficient mutant. It is also possible that differences in the kinetic rate of γ-secretase processing between palmitoylated and non-palmitoylated BTC-CTF explains the observed results. Nevertheless, similar to $p75^{NTR}$ (Underwood et al., 2008), our results indicate that palmitoylation of proBTC is a crucial post-translational modification required for efficient production of BTC-ICD.

The divergent subcellular distribution of palmitoylated BTC-ΔE compared with the non-palmitoylated BTC-ICD-Only mutant suggests that palmitoylation also influences trafficking and localization of BTC-ICD. How can these apparently distinct cellular distributions be reconciled? In contrast to other ErbB-ligand precursors, the predicted BTC-ICD has a highly conserved nine-amino-acid motif (^{146}RKRRKRKKK) that is reminiscent of a nuclear localization signal (NLS). We speculate that this putative NLS is responsible for the trafficking of BTC-ICD-Only into the nucleus, where it is retained by interactions with the nuclear architecture (Lusk et al., 2007). Protein palmitoylation is a reversible process that enables proteins to shuttle between distinct intracellular compartments (Greaves and Chamberlain, 2007; Greaves et al., 2009; Linder and Deschenes, 2006; Linder and Deschenes, 2007). Thus, for palmitoylated BTC-ICD generated from BTC-ΔE or BTC-WT, palmitoylation might provide a mechanism for recycling and trafficking of BTC-ICD to the ER and/or outer nuclear membrane (ONM), where BTC-ICD can either diffuse or be actively transported by its NLS across the nuclear pore to the inner nuclear membrane. Indeed, treatment of cells expressing BTC-ΔE with a γ-secretase inhibitor led to a reduction of BTC-ICD staining at the nuclear membrane, indicating that palmitoylated BTC-ICD is responsible, in part, for the accumulation of BTC-ICD at the nuclear membrane. Alternatively, palmitoylated BTC-ICD might act as a stable membrane-associated pool that can be released by deacetylation and sent to the nucleus in a similar manner to the BTC-ICD-Only mutant. In this context, it would be interesting to know the cellular distribution and signaling activity of palmitoylated $p75^{NTR}$-ICD and whether it undergoes rapid deacetylation (Underwood et al., 2008).

The analysis of BTC-ΔE nuclear trafficking is further complicated because both full-length BTC-ΔE and its BTC-ICD are detected in nuclear fractions and presumably both are localized at the nuclear membrane. A similar pattern is observed for BTC-WT, for which only the 19-kDa BTC isoform and BTC-ICD are detected in nuclear fractions. Recent studies have proposed that integral proteins might traffic into the nucleus using similar NLS-targeting machinery to soluble proteins (Lusk et al., 2007). Thus, similar to palmitoylated BTC-ICD, we postulate that the palmitoylated 19-kDa BTC and full-length BTC-ΔE isoforms might also recycle through the ER and/or ONM and, because they are sufficiently small, might also diffuse or be actively transported by their NLS to the INM (Lusk et al., 2007). Interestingly, the recruitment of the 19-kDa BTC isoform and full-length BTC-ΔE to nuclear fractions is also very reminiscent of the trafficking of specific HB-EGF and AR isoforms to the nuclear membrane. (Hieda et al., 2008; Isokane et al., 2008). Although it is currently unknown why these specific ligand precursor isoforms are selected for nuclear trafficking, it is interesting to note that the 19-kDa BTC isoform and full-length BTC-ΔE represent N-terminally truncated BTC isoforms are smaller than other isoforms but also lack glycosylation and the heparin-binding domain, which might exclude the larger cellular BTC isoforms from the nucleus. It will therefore be important to demonstrate whether palmitoylation, the putative NLS or other unique ER retrograde and/or nuclear sorting signals are responsible for BTC-ICD trafficking.

The striking similarities in nuclear membrane localization of BTC-ICD to those reported for select HB-EGF and AR isoforms also suggest a possible role of these BTC cleavage fragments in regulating cellular processes independent of ErbB receptors (Hieda et al., 2008; Isokane et al., 2008). Indeed, we found that the ligand-containing extracellular domain of proBTC acts in a dominant ErbB-receptor-dependent manner to enhance proliferation, whereas the BTC-ICD, when separated from the extracellular domain and overexpressed, acts to inhibit growth through a receptor-independent pathway. Although the mechanisms of growth inhibition by BTC-ICD are currently being investigated, it suggests that BTC-ICD is engaged in novel receptor-independent signaling that might regulate other cellular functions that either act in concert or in opposition to ligand-mediated receptor signaling.

In summary, we have demonstrated that proBTC is sequentially processed by ADAM10 and presenilin1/2-dependent γ-secretase to generate a BTC-ICD. Palmitoylation has been identified as a novel mechanism to regulate efficient γ-secretase-dependent processing of BTC-WT and is required for BTC-ICD recruitment to the nuclear membrane. In the IMPE pancreatic cell line, BTC-ICD led to inhibition of cell proliferation, providing the first evidence that the BTC-ICD might be involved in a unique receptor-independent signaling pathway. BTC has beneficial effects on pancreatic β-cell growth and survival and BTC gene therapy is currently being investigated as a strategy to promote β-cell regeneration and improved glucose tolerance in vivo (Chen et al., 2007; Shin et al., 2008). Thus, further characterization of BTC-ICD intracellular signaling might provide new insights into improving the efficacy of these gene-therapy approaches in the treatment of diabetes and β-cell replacement strategies.

Materials and Methods

Antibodies and reagents

The following antibodies and reagents were used: biotinylated goat anti-human BTC ectodomain antibody, mouse anti-human BTC ectodomain antibody and rat anti-mouse ADAM10 antibody (R&D Systems); rabbit anti-HA epitope tag antibody (Zymed Laboratories, Bethyl Laboratories); mouse anti-HA agarose beads (Sigma); mouse anti-GFP (Clontech); horseradish-peroxidase-conjugated donkey anti-rabbit IgG F(ab)2 fragment (Amersham Biosciences); mouse anti-actin anti-histone-2 (Millipore); and mouse anti-PolII antibody (Santa Cruz Biotechnology). Recombinant human BTC and mouse interferon-γ (IFN-γ) were purchased from R&D Systems. Ca^{2+} ionophore (A23187) was purchased from Sigma and protease inhibitor mixture was purchased from Roche Diagnostics. SuperSignal West Pico substrate, streptavidin-agarose and protein-G-agarose were obtained from Pierce. Horseradish-peroxidase-conjugated streptavidin was purchased from Jackson ImmunoResearch Laboratories. GM6001 was obtained from Chemicon International. ADAM10-selective inhibitor (GI254023X) and ADAM10/17 inhibitor (GW280264X) were generously provided by Peter Gough (GlaxoSmithKline, UK). All other inhibitors were purchased from Calbiochem.

Expression constructs, retroviral transduction and cell culture

The cDNAs encoding human *BTC* containing a C-terminal HA epitope or EGFP tag were generated as previously described (Sanderson et al., 2005). All additional proBTC mutants were generated by PCR amplification and information for the specific primer sequences can be obtained upon request. All BTC constructs were cloned into the pBM-IRES-PURO retroviral vector and stable retroviral transduction of cell lines performed as described (Sanderson et al., 2005).

The IMPE cell line (Whitehead and Robinson, 2009) was cultured as previously described (Moss et al., 2007). WT, ADAM10-deficient and presenilin-1/2-deficient MEFs (Hartmann et al., 2002; Herreman et al., 2000) and HEK293 cells were cultured at 37°C in Dulbecco's modified Eagle's medium (DMEM) plus 10% fetal bovine serum/penicillin/streptomycin/nonessential amino acids.

BTC cleavage assays

BTC cleavage assays were performed as previously described (Moss et al., 2007; Sanderson et al., 2005). For analysis of constitutive shedding, cells were cultured for 4 or 24 hours in serum-free DMEM plus 2 μM GI254023X or 0.2 μM PIX. To

stimulate BTC cleavage, cells were cultured for 1 hour in serum-free DMEM with or without 2 μM A23187. CM and cell lysates were harvested and used directly in the BTC enzyme-linked immunosorbent assay (ELISA) and/or in immunoprecipitation and western blot experiments as previously described (Sanderson et al., 2005). A specific human BTC sandwich ELISA (R&D Systems) was used to quantify BTC levels in CM and cell lysates (Moss et al., 2007; Sanderson et al., 2005).

S-palmitoylation assays

Labeling of S-palmitoylated residues was performed using an S-palmitoylation-specific acyl-biotin exchange assay as previously described (Cheng et al., 2009; Drisdel et al., 2006; Drisdel and Green, 2004). Briefly, IMPE cells expressing different BTC constructs were grown in regular growth medium, washed twice with ice-cold phosphate-buffered saline (PBS) and then lysed in lysis buffer (LB; 150 mM NaCl, 5 mM EDTA, 50 mM Tris, pH 7.2, 0.02% NaN_3, 1% TX-100, 2 mM PMSF and inhibitor cocktail) with or without 50 mM NEM (Pierce). Cell lysates were pre-cleared and immunoprecipitated with anti-HA-agarose. Immunoprecipitates were washed three times with LB without NEM to remove free NEM and then treated with 1 M hydroxylamine-HCl (Pierce) in PBS, pH 7.4, or 1 M Tris, pH 7.4, for 1 hour at room temperature (RT). Subsequently, immunoprecipitates were washed three times with LB, labeled with 1 μM EZ-Link Biotin-BMCC (Thermo Scientific) for 2 hours at RT, and again washed with LB prior to western blotting. Alternatively, bound proteins were eluted from immunoprecipitates with 10% SDS-LB and boiled for 5 minutes prior to precipitation with streptavidin-agarose (Sigma) and western blotting.

For [^{3}H]-palmitic-acid labeling, IMPE cells expressing the indicated BTC constructs were rinsed twice with DMEM and then labeled with 200 μCi/ml of [^{3}H]-palmitic acid (Perkin Elmer) for 6 hours at 37°C. Cell lysates were immunoprecipitated with the anti-HA agarose, separated on 10-20% Tris/Tricine {*N*-[2-hydroxy-1,1-bis(hydroxymethyl)ethyl]glycine} gradient gel, transferred to Hybond nitrocellulose (Amersham Biosciences), and either immunoblotted with specific antibodies or membranes were dried and analyzed by autoradiography.

Elution of BTC-ICD from membrane fractions by hydroxylamine treatment

IMPE cells expressing different BTC constructs were grown in regular growth medium, washed twice with ice-cold PBS and then homogenized in 1 M hydroxylamine-HCl (Pierce) in PBS, pH 7.4, or 1 M Tris, pH 7.4, for 1 hour at RT. Homogenates were spun at 100,000 ***g*** and pelleted membranes were lysed in LB. Both lysates and supernatants were immunoprecipitated with anti-HA agarose and analyzed by western blotting.

Purification of nuclear proteins

Separation of cell nuclei and membrane/cytosol was performed as previously described (Lee and Green, 1990) with the following modifications. IMPE cells expressing different BTC constructs were trypsinized and washed twice with cold PBS and once with 20 ml of buffer A (10 mM Tris-HCl, pH 7.4, 8.3 mM KCl, 1.5 mM $MgSO_4$, 1.3 mM NaCl). Cells were then swollen on ice for 30 minutes in buffer A. Nuclei/membranes and cytosol were separated by passing the suspension eight times through a 23-gauge needle followed by 20 rounds through a glass-glass homogenizer. Nuclei and membranes were pelleted by centrifugation at 3000 ***g*** for 10 minutes. Supernatant (cytosolic fraction) was cleared by centrifugation at 10,000 ***g***. Proteins in the cytosolic fractions were then precipitated by addition of trichloracetic acid (TCA) at a final concentration of 10%, incubated on ice for 30 minutes and pelleted through centrifugation for another 30 minutes at 10,000 ***g*** and 4°C. Pellets were washed twice with diethyl ether, dried overnight and finally re-suspended in sample buffer.

Nuclei and membranes were re-suspended in 10 ml of buffer B (buffer A supplemented with 0.5% NP-40 and 1 mM PMSF) and separated by passing the suspension again eight times through a 23-gauge needle followed by 20 rounds through a glass-glass homogenizer. The homogenate was spun for 10 minutes at 1000 ***g*** to pellet the nuclei. The supernatant (membrane fraction) was precipitated with TCA as described above. The nuclear pellet was re-suspended in 10 ml of buffer C (buffer A containing 1 mM PMSF), purity of nuclei was verified under a microscope, and centrifuged at 1000 ***g*** for 10 minutes. The pellet was re-suspended in buffer S1 (0.25 M sucrose, 1.5 mM $MgSO_4$, 1 mM PMSF), layered on top of 15 ml buffer S2 (0.88 M sucrose, 0.05 mM $MgSO_4$) and centrifuged for 15 minutes at 2500 ***g***. The sediment containing the purified nuclei was re-suspended in 120 μl of buffer S3 (0.34 M sucrose, 0.05 mM $MgSO_4$, 1 mM PMSF), shortly sonicated and prepared for western blotting by addition of SDS-PAGE sample buffer and analyzed in western blot with antibodies against HA, tubulin (as a cytosolic marker) and RNA polymerase II (PolII, as a nuclear marker). Alternatively, cells were swollen on ice for 30 minutes in 10 ml of buffer A centrifuged at 660 ***g*** for 5 minutes and re-suspended in 10 ml of buffer B. The suspension was passed eight times through a 23-gauge needle followed by 20 rounds through a glass-glass homogenizer. Nuclei were pelleted by centrifugation at 1000 ***g*** and further processed as described above. Proteins in the supernatant (containing membrane and cytosolic proteins) were precipitated with TCA as described and resuspended in SDS-PAGE sample buffer.

Confocal microscopy

Cells grown on collagen-coated coverslips were fixed with 2% paraformaldehyde (PFA), permeabilized with 100% methanol or treated with PBS/0.1% TX-100, blocked with 5% normal donkey serum in PBS and then stained with a rabbit anti-HA antibody (Zymed) followed by Cy3-conjugated secondary antibody (Jackson ImmunoResearch). For visualization of DNA, cells were stained with Hoechst 33258 (DAPI) stain (Sigma). All immunofluorescence imaging was analyzed using an Olympus Fluoview 500 confocal microscope.

Cell-proliferation assay

IMPE cells expressing the indicated BTC constructs were plated at 5×10^4 cells/well in six-well plates and grown overnight in regular growth media without IFN-γ at 37°C. Cells were trypsinized the next day and counted in a coulter counter (Beckman). Counts were defined as 100%. Medium was changed to DMEM containing 0.5% FBS and cell numbers were counted again after 24, 48 and 72 hours.

Data analysis

All experiments were repeated at least three times with similar results, and a representative figure is presented. Values for each experiment are expressed as the means ± s.e.m. of quadruplicate determinations.

This study was supported by JDRF (5-2007-969) and NIH (DK63633) grants to P.J.D. This work utilized cores supported by the MDRTC (NIH 5P60 DK020572) and University of Michigan Cancer Center (NIH 5P30 CA46592). We are grateful to Deiter Hartmann, Paul Saftig and Bart de Strooper for generously providing the ADAM10-deficient and presenilin-1/2-deficient MEF cell lines. Deposited in PMC for release after 12 months.

Supplementary material available online at
http://jcs.biologists.org/cgi/content/full/123/13/2319/DC1

References

Bao, J., Wolpowitz, D., Role, L. W. and Talmage, D. A. (2003). Back signaling by the Nrg-1 intracellular domain. *J. Cell Biol.* **161**, 1133-1141.

Bao, J., Lin, H., Ouyang, Y., Lei, D., Osman, A., Kim, T. W., Mei, L., Dai, P., Ohlemiller, K. K. and Ambron, R. T. (2004). Activity-dependent transcription regulation of PSD-95 by neuregulin-1 and Eos. *Nat. Neurosci.* **7**, 1250-1258.

Baron, M. (2003). An overview of the Notch signalling pathway. *Semin. Cell Dev. Biol.* **14**, 113-119.

Blobel, C. P. (2005). ADAMs: key components in EGFR signalling and development. *Nat. Rev. Mol. Cell Biol.* **6**, 32-43.

Brown, C. L., Coffey, R. J. and Dempsey, P. J. (2001). The proamphiregulin cytoplasmic domain is required for basolateral sorting, but is not essential for constitutive or stimulus-induced processing in polarized Madin-Darby canine kidney cells. *J. Biol. Chem.* **276**, 29538-29549.

Chen, S., Ding, J., Yu, C., Yang, B., Wood, D. R. and Grayburn, P. A. (2007). Reversal of streptozotocin-induced diabetes in rats by gene therapy with betacellulin and pancreatic duodenal homeobox-1. *Gene Ther.* **14**, 1102-1110.

Cheng, H., Vetrivel, K. S., Drisdel, R. C., Meckler, X., Gong, P., Leem, J. Y., Li, T., Carter, M., Chen, Y., Nguyen, P. et al. (2009). S-palmitoylation of gamma-secretase subunits nicastrin and APH-1. *J. Biol. Chem.* **284**, 1373-1384.

Citri, A. and Yarden, Y. (2006). EGF-ERBB signalling: towards the systems level. *Nat. Rev. Mol. Cell Biol.* **7**, 505-516.

De Strooper, B., Annaert, W., Cupers, P., Saftig, P., Craessaerts, K., Mumm, J. S., Schroeter, E. H., Schrijvers, V., Wolfe, M. S., Ray, W. J. et al. (1999). A presenilin-1-dependent gamma-secretase-like protease mediates release of Notch intracellular domain. *Nature* **398**, 518-522.

Dempsey, P. J. and Coffey, R. J. (1994). Basolateral targeting and efficient consumption of transforming growth factor-alpha when expressed in Madin-Darby canine kidney cells. *J. Biol. Chem.* **269**, 16878-16889.

Dempsey, P. J., Meise, K. S., Yoshitake, Y., Nishikawa, K. and Coffey, R. J. (1997). Apical enrichment of human EGF precursor in Madin-Darby canine kidney cells involves preferential basolateral ectodomain cleavage sensitive to a metalloprotease inhibitor. *J. Cell Biol.* **138**, 747-758.

Dempsey, P. J., Garton, K. and Raines, E. W. (2002). Emerging roles of TACE as a key protease in ErbB ligand shedding. *Mol. Interv.* **2**, 136-141.

Dempsey, P. J., Meise, K. S. and Coffey, R. J. (2003). Basolateral sorting of transforming growth factor-alpha precursor in polarized epithelial cells: characterization of cytoplasmic domain determinants. *Exp. Cell Res.* **285**, 159-174.

Dong, J. and Wiley, H. S. (2000). Trafficking and proteolytic release of epidermal growth factor receptor ligands are modulated by their membrane-anchoring domains. *J. Biol. Chem.* **275**, 557-564.

Dong, J., Opresko, L. K., Dempsey, P. J., Lauffenburger, D. A., Coffey, R. J. and Wiley, H. S. (1999a). Metalloprotease-mediated ligand release regulates autocrine signaling through the epidermal growth factor receptor. *Proc. Natl. Acad. Sci. USA* **96**, 6235-6240.

Dong, J., Opresko, L. K., Dempsey, P. J., Lauffenburger, D. A., Coffey, R. J. and Wiley, H. S. (1999b). Metalloprotease-mediated ligand release regulates autocrine

signaling through the epidermal growth factor receptor. *Proc. Natl. Acad. Sci. USA* **96**, 6235-6240.

Dong, J., Opresko, L. K., Chrisler, W., Orr, G., Quesenberry, R. D., Lauffenburger, D. A. and Wiley, H. S. (2005). The membrane-anchoring domain of epidermal growth factor receptor ligands dictates their ability to operate in juxtacrine mode. *Mol. Biol. Cell* **16**, 2984-2998.

Drisdel, R. C. and Green, W. N. (2004). Labeling and quantifying sites of protein palmitoylation. *Biotechniques* **36**, 276-285.

Drisdel, R. C., Alexander, J. K., Sayeed, A. and Green, W. N. (2006). Assays of protein palmitoylation. *Methods* **40**, 127-134.

Dunbar, A. J. and Goddard, C. (2000). Structure-function and biological role of betacellulin. *Int. J. Biochem. Cell Biol.* **32**, 805-815.

Dunbar, A. J., Priebe, I. K., Sanderson, M. P. and Goddard, C. (2001). Purification and molecular characterization of recombinant rat betacellulin. *J. Mol. Endocrinol.* **27**, 239-247.

Ebinu, J. O. and Yankner, B. A. (2002). A RIP tide in neuronal signal transduction. *Neuron* **34**, 499-502.

Ferber, E. C., Kajita, M., Wadlow, A., Tobiansky, L., Niessen, C., Ariga, H., Daniel, J. and Fujita, Y. (2008). A role for the cleaved cytoplasmic domain of E-cadherin in the nucleus. *J. Biol. Chem.* **283**, 12691-12700.

Franklin, J. L., Yoshiura, K., Dempsey, P. J., Bogatcheva, G., Jeyakumar, L., Meise, K. S., Pearsall, R. S., Threadgill, D. and Coffey, R. J. (2005). Identification of MAGI-3 as a transforming growth factor-alpha tail binding protein. *Exp. Cell Res.* **303**, 457-470.

Gil, C., Cubi, R. and Aguilera, J. (2007). Shedding of the p75NTR neurotrophin receptor is modulated by lipid rafts. *FEBS Lett.* **581**, 1851-1858.

Glogowska, A., Pyka, J., Kehlen, A., Los, M., Perumal, P., Weber, E., Cheng, S. Y., Hoang-Vu, C. and Klonisch, T. (2008). The cytoplasmic domain of proEGF negatively regulates motility and elastinolytic activity in thyroid carcinoma cells. *Neoplasia* **10**, 1120-1130.

Greaves, J. and Chamberlain, L. H. (2007). Palmitoylation-dependent protein sorting. *J. Cell Biol.* **176**, 249-254.

Greaves, J., Prescott, G. R., Gorleku, O. A. and Chamberlain, L. H. (2009). The fat controller: roles of palmitoylation in intracellular protein trafficking and targeting to membrane microdomains (Review). *Mol. Membr. Biol.* **26**, 67-79.

Hartmann, D., de Strooper, B., Serneels, L., Craessaerts, K., Herreman, A., Annaert, W., Umans, L., Lubke, T., Lena Illert, A., von Figura, K. et al. (2002). The disintegrin/metalloprotease ADAM 10 is essential for Notch signalling but not for alpha-secretase activity in fibroblasts. *Hum. Mol. Genet.* **11**, 2615-2624.

Hass, M. R., Sato, C., Kopan, R. and Zhao, G. (2009). Presenilin: RIP and beyond. *Semin. Cell Dev. Biol.* **20**, 201-210.

Herreman, A., Serneels, L., Annaert, W., Collen, D., Schoonjans, L. and De Strooper, B. (2000). Total inactivation of gamma-secretase activity in presenilin-deficient embryonic stem cells. *Nat. Cell Biol.* **2**, 461-462.

Hieda, M., Isokane, M., Koizumi, M., Higashi, C., Tachibana, T., Shudou, M., Taguchi, T., Hieda, Y. and Higashiyama, S. (2008). Membrane-anchored growth factor, HB-EGF, on the cell surface targeted to the inner nuclear membrane. *J. Cell Biol.* **180**, 763-769.

Higashiyama, S., Iwabuki, H., Morimoto, C., Hieda, M., Inoue, H. and Matsushita, N. (2008). Membrane-anchored growth factors, the epidermal growth factor family: beyond receptor ligands. *Cancer Sci.* **99**, 214-220.

Imhof, I., Gasper, W. J. and Derynck, R. (2008). Association of tetraspanin CD9 with transmembrane TGF{alpha} confers alterations in cell-surface presentation of TGF{alpha} and cytoskeletal organization. *J. Cell Sci.* **121**, 2265-2274.

Isokane, M., Hieda, M., Hirakawa, S., Shudou, M., Nakashiro, K., Hashimoto, K., Hamakawa, H. and Higashiyama, S. (2008). Plasma-membrane-anchored growth factor pro-amphiregulin binds A-type lamin and regulates global transcription. *J. Cell Sci.* **121**, 3608-3618.

Kinugasa, Y., Hieda, M., Hori, M. and Higashiyama, S. (2007). The carboxyl-terminal fragment of pro-HB-EGF reverses Bcl6-mediated gene repression. *J. Biol. Chem.* **282**, 14797-14806.

Klonisch, T., Glogowska, A., Gratao, A. A., Grzech, M., Nistor, A., Torchia, M., Weber, E., de Angelis, M. H., Rathkolb, B., Cuong, H. V. et al. (2009). The C-terminal cytoplasmic domain of human proEGF is a negative modulator of body and organ weights in transgenic mice. *FEBS Lett.* **583**, 1349-1357.

Lee, K. A. and Green, M. R. (1990). Small-scale preparation of extracts from radiolabeled cells efficient in pre-mRNA splicing. *Methods Enzymol.* **181**, 20-30.

Linder, M. E. and Deschenes, R. J. (2006). Protein palmitoylation. *Methods* **40**, 125-126.

Linder, M. E. and Deschenes, R. J. (2007). Palmitoylation: policing protein stability and traffic. *Nat. Rev. Mol. Cell Biol.* **8**, 74-84.

Lusk, C. P., Blobel, G. and King, M. C. (2007). Highway to the inner nuclear membrane: rules for the road. *Nat. Rev. Mol. Cell Biol.* **8**, 414-420.

Maddon, P. J., Littman, D. R., Godfrey, M., Maddon, D. E., Chess, L. and Axel, R. (1985). The isolation and nucleotide sequence of a cDNA encoding the T cell surface protein T4: a new member of the immunoglobulin gene family. *Cell* **42**, 93-104.

Matthews, V., Schuster, B., Schutze, S., Bussmeyer, I., Ludwig, A., Hundhausen, C., Sadowski, T., Saftig, P., Hartmann, D., Kallen, K. J. et al. (2003). Cellular cholesterol depletion triggers shedding of the human interleukin-6 receptor by ADAM10 and ADAM17 (TACE). *J. Biol. Chem.* **278**, 38829-38839.

Moss, M. L., Bomar, M., Liu, Q., Sage, H., Dempsey, P., Lenhart, P. M., Gillispie, P. A., Stoeck, A., Wildeboer, D., Bartsch, J. W. et al. (2007). The ADAM10 prodomain is a specific inhibitor of ADAM10 proteolytic activity and inhibits cellular shedding events. *J. Biol. Chem.* **282**, 35712-35721.

Mumm, J. S., Schroeter, E. H., Saxena, M. T., Griesemer, A., Tian, X., Pan, D. J., Ray, W. J. and Kopan, R. (2000). A ligand-induced extracellular cleavage regulates gamma-secretase-like proteolytic activation of Notch1. *Mol. Cell* **5**, 197-206.

Murakami, D., Okamoto, I., Nagano, O., Kawano, Y., Tomita, T., Iwatsubo, T., De Strooper, B., Yumoto, E. and Saya, H. (2003). Presenilin-dependent gamma-secretase activity mediates the intramembranous cleavage of CD44. *Oncogene* **22**, 1511-1516.

Nanba, D., Mammoto, A., Hashimoto, K. and Higashiyama, S. (2003). Proteolytic release of the carboxy-terminal fragment of proHB-EGF causes nuclear export of PLZF. *J. Cell Biol.* **163**, 489-502.

Ohtsu, H., Dempsey, P. J. and Eguchi, S. (2006). ADAMs as mediators of EGF receptor transactivation by G protein-coupled receptors. *Am. J. Physiol. Cell Physiol.* **291**, C1-C10.

Parkin, E. and Harris, B. (2009). A disintegrin and metalloproteinase (ADAM)-mediated ectodomain shedding of ADAM10. *J. Neurochem.* **108**, 1464-1479.

Peschon, J. J., Slack, J. L., Reddy, P., Stocking, K. L., Sunnarborg, S. W., Lee, D. C., Russell, W. E., Castner, B. J., Johnson, R. S., Fitzner, J. N. et al. (1998a). An essential role for ectodomain shedding in mammalian development. *Science* **282**, 1281-1284.

Pyka, J., Glogowska, A., Dralle, H., Hoang-Vu, C. and Klonisch, T. (2005). Cytoplasmic domain of proEGF affects distribution and post-translational modification of microtubuli and increases microtubule-associated proteins 1b and 2 production in human thyroid carcinoma cells. *Cancer Res.* **65**, 1343-1351.

Riedle, S., Kiefel, H., Gast, D., Bondong, S., Wolterink, S., Gutwein, P. and Altevogt, P. (2009). Nuclear translocation and signaling of L1-CAM in human carcinoma cells requires ADAM10 and presenilin/gamma-secretase activity. *Biochem. J.* **420**, 391-402.

Riese, D. J., 2nd, Bermingham, Y., van Raaij, T. M., Buckley, S., Plowman, G. D. and Stern, D. F. (1996). Betacellulin activates the epidermal growth factor receptor and erbB-4, and induces cellular response patterns distinct from those stimulated by epidermal growth factor or neuregulin-beta. *Oncogene* **12**, 345-353.

Sahin, U., Weskamp, G., Kelly, K., Zhou, H. M., Higashiyama, S., Peschon, J., Hartmann, D., Saftig, P. and Blobel, C. P. (2004). Distinct roles for ADAM10 and ADAM17 in ectodomain shedding of six EGFR ligands. *J. Cell Biol.* **164**, 769-779.

Sanderson, M., Erickson, S., Gough, P., Garton, K., Wille, P., Raines, E., Dunbar, A. and Dempsey, P. (2004). ADAM10 mediates ectodomain shedding of the betacullulin precursor activated by p-aminophenylmercuric acetate and extracellular calcium influx. *J. Biol. Chem.* **230**, 1826-1837.

Sanderson, M. P., Erickson, S. N., Gough, P. J., Garton, K. J., Wille, P. T., Raines, E. W., Dunbar, A. J. and Dempsey, P. J. (2005). ADAM10 mediates ectodomain shedding of the betacellulin precursor activated by p-aminophenylmercuric acetate and extracellular calcium influx. *J. Biol. Chem.* **280**, 1826-1837.

Sanderson, M. P., Abbott, C. A., Tada, H., Seno, M., Dempsey, P. J. and Dunbar, A. J. (2006a). Hydrogen peroxide and endothelin-1 are novel activators of betacellulin ectodomain shedding. *J. Cell Biochem.* **99**, 609-623.

Sanderson, M. P., Dempsey, P. J. and Dunbar, A. J. (2006b). Control of ErbB signaling through metalloprotease mediated ectodomain shedding of EGF-like factors. *Growth Factors* **24**, 121-136.

Selkoe, D. and Kopan, R. (2003). Notch and Presenilin: regulated intramembrane proteolysis links development and degeneration. *Annu. Rev. Neurosci.* **26**, 565-597.

Shi, W., Fan, H., Shum, L. and Derynck, R. (2000). The tetraspanin CD9 associates with transmembrane TGF-alpha and regulates TGF-alpha-induced EGF receptor activation and cell proliferation. *J. Cell Biol.* **148**, 591-602.

Shin, S., Li, N., Kobayashi, N., Yoon, J. W. and Jun, H. S. (2008). Remission of diabetes by beta-cell regeneration in diabetic mice treated with a recombinant adenovirus expressing betacellulin. *Mol. Ther.* **16**, 854-861.

Shum, L., Reeves, S. A., Kuo, A. C., Fromer, E. S. and Derynck, R. (1994). Association of the transmembrane TGF-alpha precursor with a protein kinase complex. *J. Cell Biol.* **125**, 903-916.

Shum, L., Turck, C. W. and Derynck, R. (1996). Cysteines 153 and 154 of transmembrane transforming growth factor-alpha are palmitoylated and mediate cytoplasmic protein association. *J. Biol. Chem.* **271**, 28502-28508.

Steinhilb, M. L., Turner, R. S. and Gaut, J. R. (2001). The protease inhibitor, MG132, blocks maturation of the amyloid precursor protein Swedish mutant preventing cleavage by beta-Secretase. *J. Biol. Chem.* **276**, 4476-4484.

Stoeck, A., Keller, S., Riedle, S., Sanderson, M. P., Runz S, Le Naour, F., Gutwein, P., Ludwig, A., Rubinstein, E. and Altevogt, P. (2006). A role for exosomes in the constitutive and stimulus-induced ectodomain cleavage of L1 and CD44. *Biochem. J.* **393**, 609-618.

Sunnarborg, S. W., Hinkle, C. L., Stevenson, M., Russell, W. E., Raska, C. S., Peschon, J. J., Castner, B. J., Gerhart, M. J., Paxton, R. J., Black, R. A. et al. (2002). Tumor necrosis factor-alpha converting enzyme (TACE) regulates epidermal growth factor receptor ligand availability. *J. Biol. Chem.* **277**, 12838-12845.

Suzuki, M., Raab, G., Moses, M. A., Fernandez, C. A. and Klagsbrun, M. (1997). Matrix metalloproteinase-3 releases active heparin-binding EGF-like growth factor by cleavage at a specific juxtamembrane site. *J. Biol. Chem.* **272**, 31730-31737.

Sweeney, C., Lai, C., Riese, D. J., 2nd, Diamonti, A. J., Cantley, L. C. and Carraway, K. L., 3rd (2000). Ligand discrimination in signaling through an ErbB4 receptor homodimer. *J. Biol. Chem.* **275**, 19803-19807.

Tousseyn, T., Thathiah, A., Jorissen, E., Raemaekers, T., Konietzko, U., Reiss, K., Maes, E., Snellinx, A., Serneels, L., Nyabi, O. et al. (2009). ADAM10, the rate-limiting protease of regulated intramembrane proteolysis of Notch and other proteins, is processed by ADAMS-9, ADAMS-15, and the gamma-secretase. *J. Biol. Chem.* **284**, 11738-1747.

Underwood, C. K., Reid, K., May, L. M., Bartlett, P. F. and Coulson, E. J. (2008). Palmitoylation of the C-terminal fragment of p75(NTR) regulates death signaling and is required for subsequent cleavage by gamma-secretase. *Mol. Cell. Neurosci.* **37**, 346-358.

Urra, S., Escudero, C. A., Ramos, P., Lisbona, F., Allende, E., Covarrubias, P., Parraguez, J. I., Zampieri, N., Chao, M. V., Annaert, W. et al. (2007). TrkA receptor activation by nerve growth factor induces shedding of the p75 neurotrophin receptor followed by endosomal gamma-secretase-mediated release of the p75 intracellular domain. *J. Biol. Chem.* **282**, 7606-7615.

Vetrivel, K. S., Cheng, H., Lin, W., Sakurai, T., Li, T., Nukina, N., Wong, P. C., Xu, H. and Thinakaran, G. (2004). Association of gamma-secretase with lipid rafts in post-Golgi and endosome membranes. *J. Biol. Chem.* **279**, 44945-44954.

Vetrivel, K. S., Cheng, H., Kim, S. H., Chen, Y., Barnes, N. Y., Parent, A. T., Sisodia, S. S. and Thinakaran, G. (2005). Spatial segregation of gamma-secretase and substrates in distinct membrane domains. *J. Biol. Chem.* **280**, 25892-25900.

von Tresckow, B., Kallen, K. J., von Strandmann, E. P., Borchmann, P., Lange, H., Engert, A. and Hansen, H. P. (2004). Depletion of cellular cholesterol and lipid rafts increases shedding of CD30. *J. Immunol.* **172**, 4324-4331.

Wang, X., Mizushima, H., Adachi, S., Ohishi, M., Iwamoto, R. and Mekada, E. (2006). Cytoplasmic domain phosphorylation of heparin-binding EGF-like growth factor. *Cell Struct. Funct.* **31**, 15-27.

Whitehead, R. H. and Robinson, P. S. (2009). Establishment of conditionally immortalized epithelial cell lines from the intestinal tissue of adult normal and transgenic mice. *Am. J. Physiol. Gastrointest. Liver Physiol.* **296**, G455-G460.

Wolfe, M. S. and Kopan, R. (2004). Intramembrane proteolysis: theme and variations. *Science* **305**, 1119-1123.

Yamazaki, S., Iwamoto, R., Saeki, K., Asakura, M., Takashima, S., Yamazaki, A., Kimura, R., Mizushima, H., Moribe, H., Higashiyama, S. et al. (2003). Mice with defects in HB-EGF ectodomain shedding show severe developmental abnormalities. *J. Cell Biol.* **163**, 469-475.

Yarden, Y. (2001). The EGFR family and its ligands in human cancer. signalling mechanisms and therapeutic opportunities. *Eur. J. Cancer* **37**, S3-S8.

Zhang, L., Song, L. and Parker, E. M. (1999). Calpain inhibitor I increases beta-amyloid peptide production by inhibiting the degradation of the substrate of gamma-secretase. Evidence that substrate availability limits beta-amyloid peptide production. *J. Biol. Chem.* **274**, 8966-8972.

Journal of Cell Science

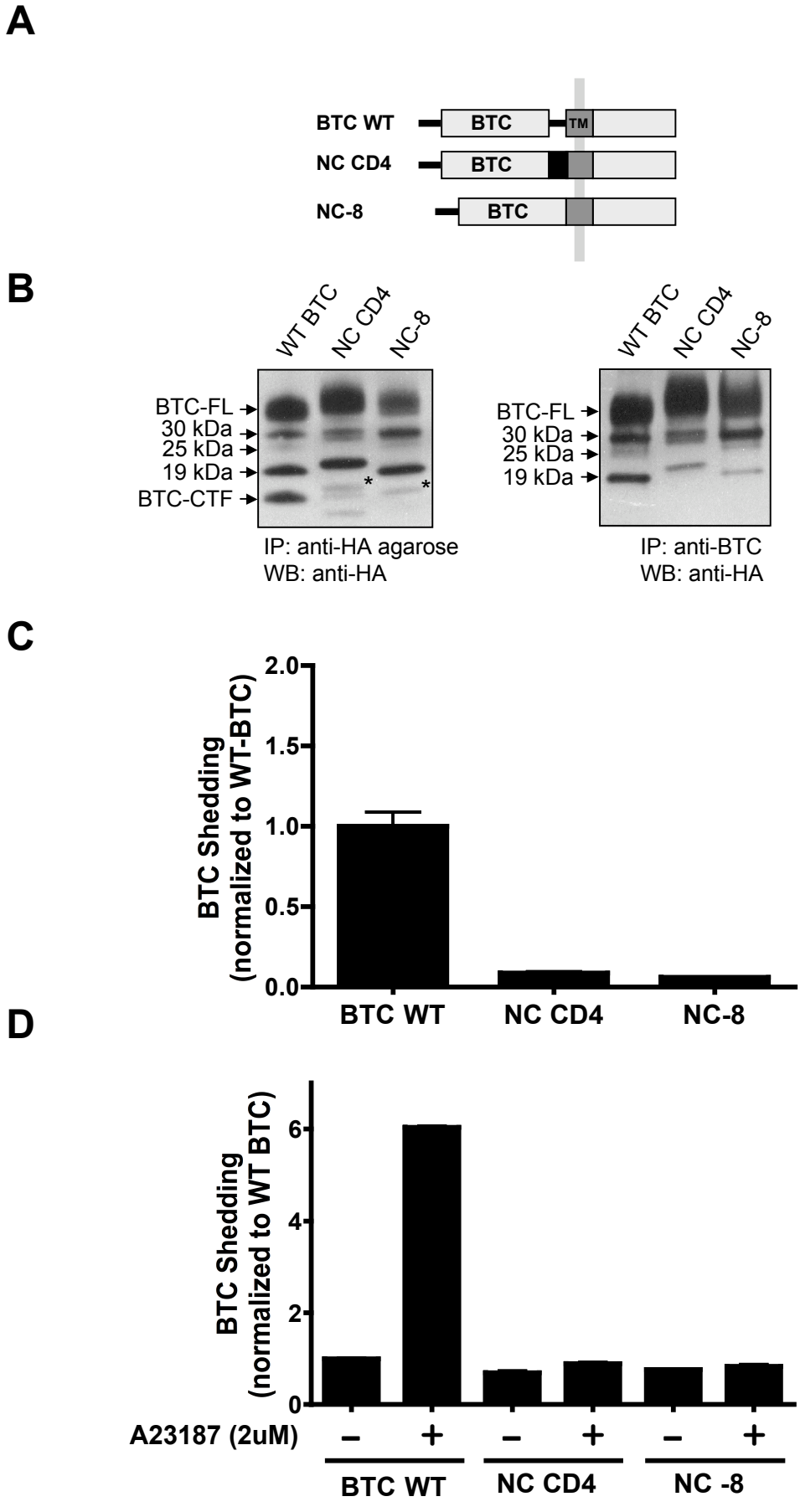
A
BTC WT
BTC
TM
NC CD4
BTC
NC-8
BTC
B
WT BTC
NC CD4
NC-8
BTC-FL
30 kDa
25 kDa
19 kDa
BTC-CTF
IP: anti-HA agarose
WB: anti-HA
WT BTC
NC CD4
NC-8
BTC-FL
30 kDa
25 kDa
19 kDa
IP: anti-BTC
WB: anti-HA
C
BTC Shedding
(normalized to WT-BTC)
2.0
1.5
1.0
0.5
0.0
BTC WT
NC CD4
NC-8
D
BTC Shedding
(normalized to WT BTC)
6
4
2
0
A23187 (2uM)
–
+
–
+
–
+
BTC WT
NC CD4
NC -8

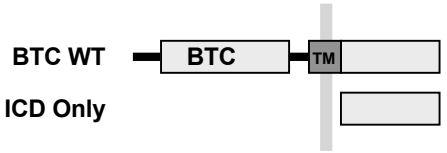
BTC WT
BTC
TM
ICD Only

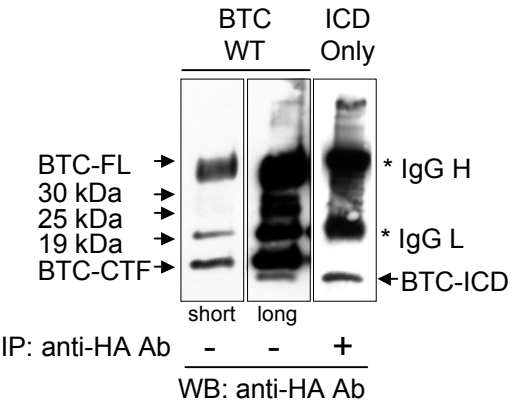
BTC
WT
ICD
Only
BTC-FL
30 kDa
25 kDa
19 kDa
BTC-CTF
* IgG H
* IgG L
BTC-ICD
short
long
IP: anti-HA Ab
-
-
+
WB: anti-HA Ab

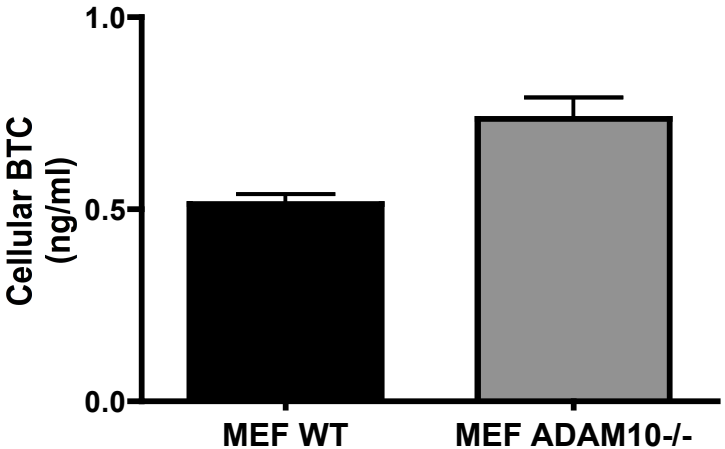
1.0
0.5
0.0
Cellular BTC
(ng/ml)
MEF WT
MEF ADAM10-/-

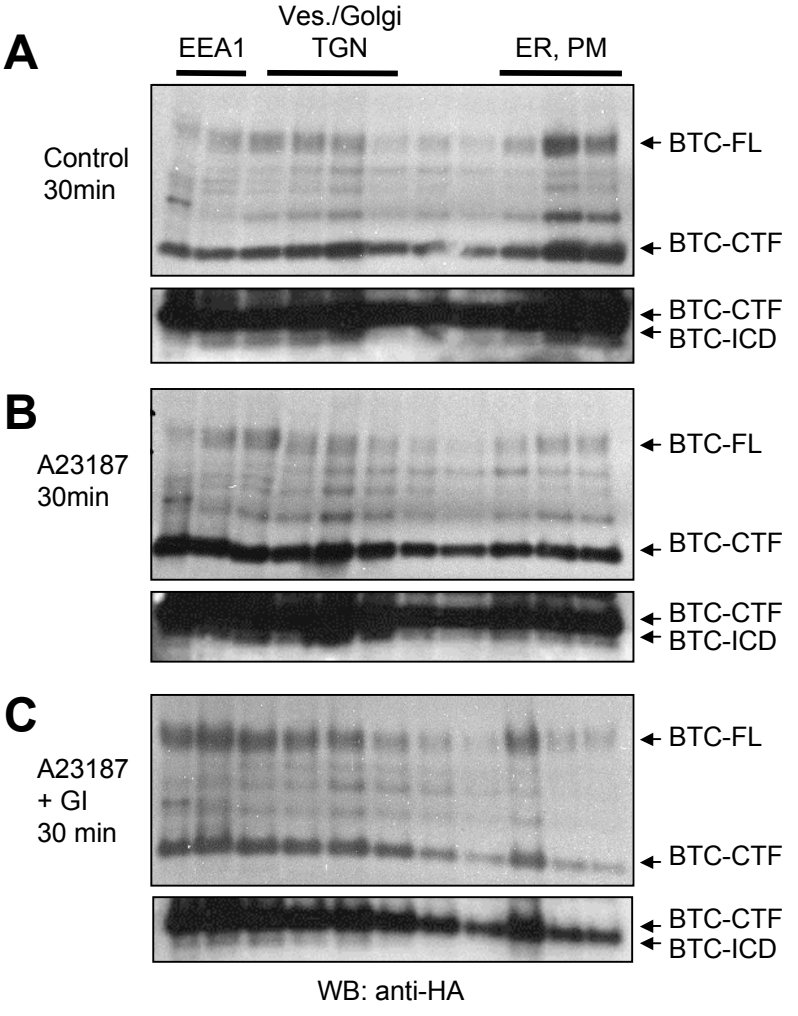
A
Ves./Golgi
EEA1
TGN
ER, PM
Control
30min
BTC-FL
BTC-CTF
BTC-CTF
BTC-ICD
B
A23187
30min
BTC-FL
BTC-CTF
BTC-CTF
BTC-ICD
C
A23187
+ GI
30 min
BTC-FL
BTC-CTF
BTC-CTF
BTC-ICD
WB: anti-HA

A

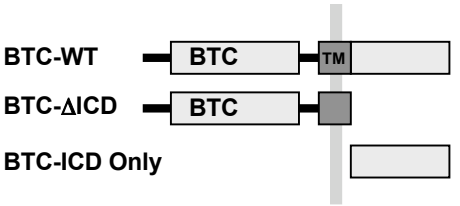
BTC-WT
BTC
TM
BTC-ΔICD
BTC
BTC-ICD Only

B

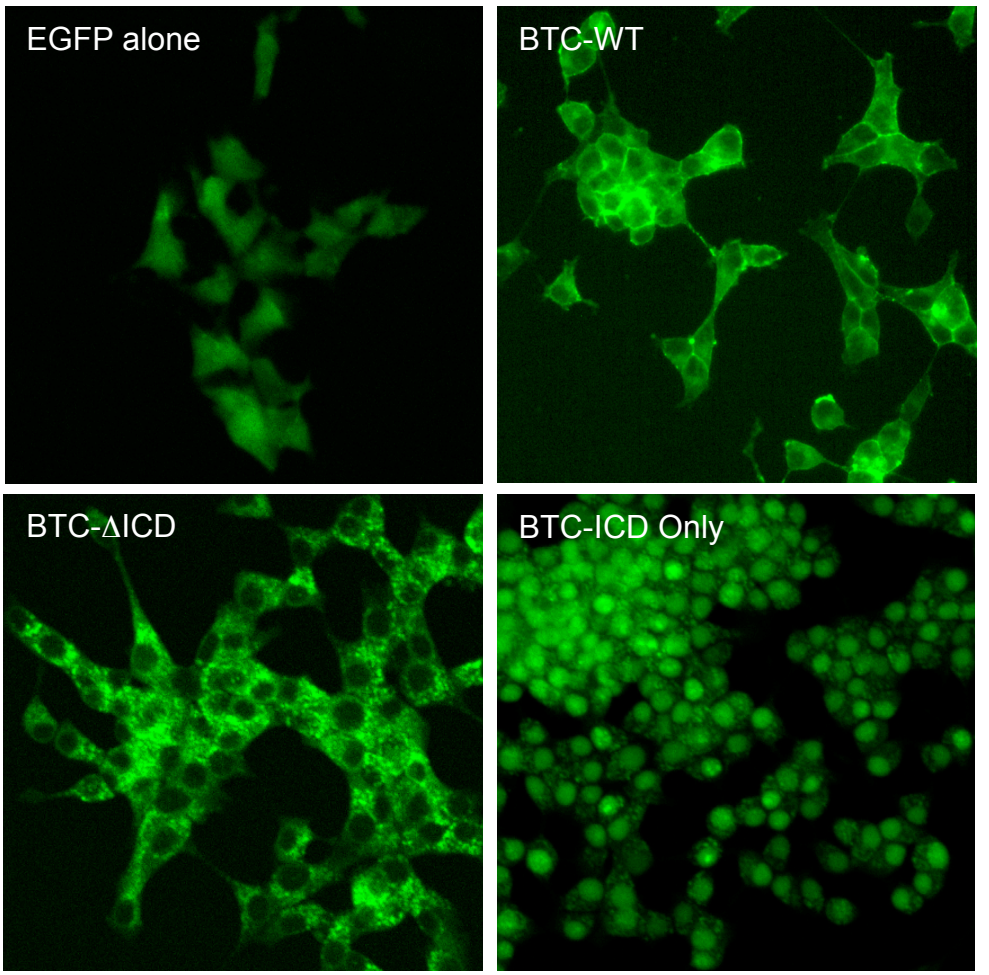
EGFP alone
BTC-WT
BTC-ΔICD
BTC-ICD Only

C

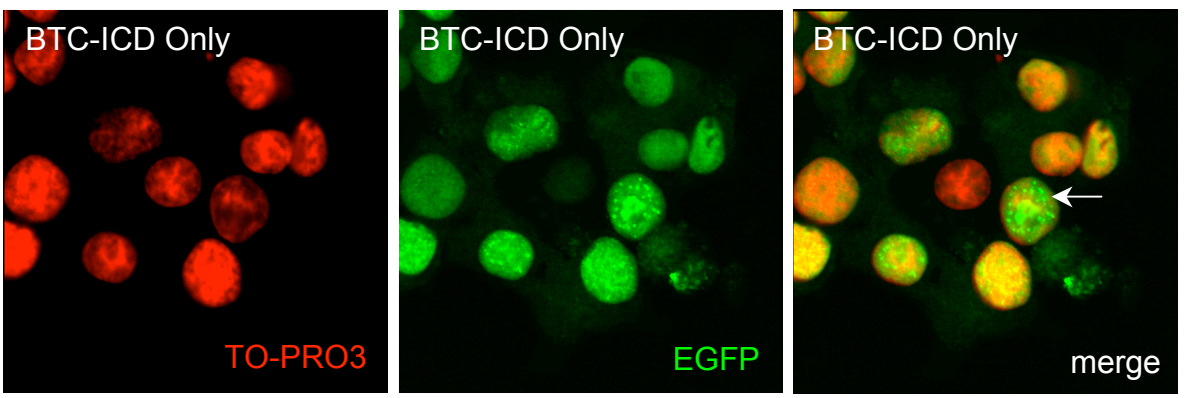
BTC-ICD Only
TO-PRO3
BTC-ICD Only
EGFP
BTC-ICD Only
merge

A

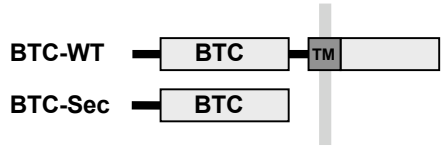
BTC-WT
BTC
TM
BTC-Sec
BTC

B

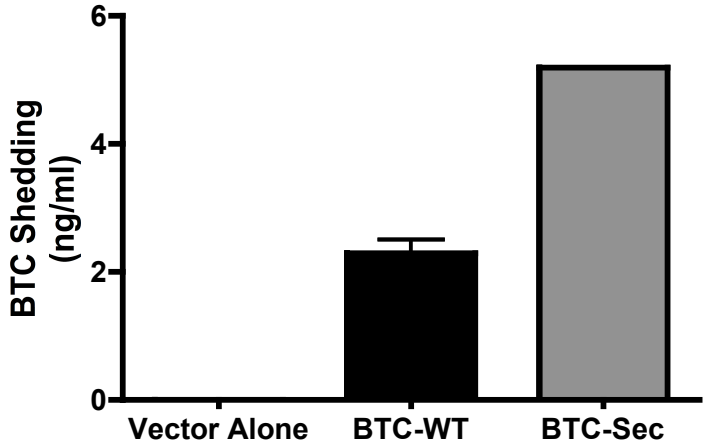
BTC Shedding
(ng/ml)
6
4
2
0
Vector Alone
BTC-WT
BTC-Sec

C

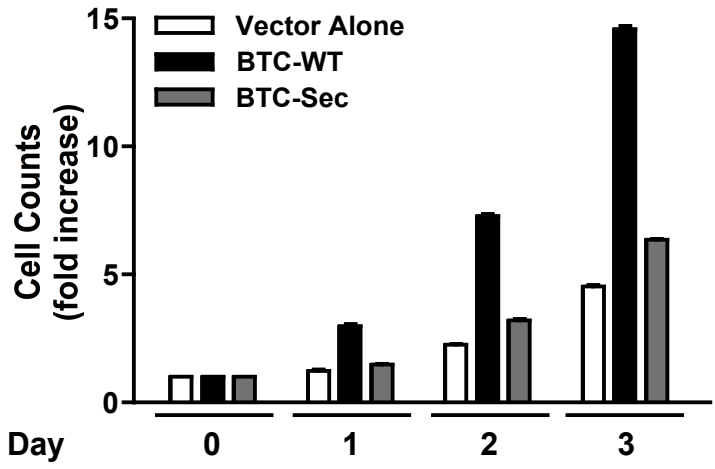
Cell Counts
(fold increase)
15
10
5
0
Vector Alone
BTC-WT
BTC-Sec
Day
0
1
2
3